

Biogeosciences Discussions is the access reviewed discussion forum of *Biogeosciences*

**Phytoplankton
optical models with
two layered spheres**

S. Bernard et al.

Simulating the optical properties of phytoplankton cells using a two-layered spherical geometry

S. Bernard^{1,2}, **T. A. Probyn**³, and **A. Quirantes**⁴

¹Department of Oceanography, University of Cape Town, Private Bag, Rondebosch 7700
Cape Town, South Africa

²Council for Scientific and Industrial Research, 11 Jan Cilliers Street, Stellenbosch,
South Africa

³Marine and Coastal Management, Private Bag X2, Rogge Bay 8012, Cape Town,
South Africa

⁴Departamento de Física Aplicada, Facultad de Ciencias, Universidad de Granada, 18071
Granada, Spain

Received: 7 October 2008 – Accepted: 12 October 2008 – Published: 30 January 2009

Correspondence to: S. Bernard (sbernard@csir.co.za)

Published by Copernicus Publications on behalf of the European Geosciences Union.

Title Page

Abstract

Introduction

Conclusions

References

Tables

Figures

◀

▶

◀

▶

Back

Close

Full Screen / Esc

Printer-friendly Version

Interactive Discussion



Abstract

Effective use of ocean colour and other bio-optical observations is dependent upon an ability to understand and characterise the angular scattering properties of phytoplankton populations. The two-layered sphere appears to offer the simplest heterogeneous geometry capable of simulating the observed angular scattering of phytoplankton cells. A study is made of the two-layered spherical model for the simulation of the inherent optical properties of algal populations, with a particular focus on backscattering as causal to ocean colour. Homogenous and two-layered volume-equivalent single particle models are used to examine the effects of varying cellular geometry, chloroplast volume, and complex refractive index on optical efficiency factors. A morphology with a chloroplast layer surrounding the cytoplasm is shown to be optimal for algal cell simulation. Appropriate chloroplast volume and refractive index ranges, and means of determining complex refractive indices for cellular chloroplast and cytoplasm material, are discussed with regard to available literature. The approach is expanded to polydispersed populations using equivalent size distribution models: to demonstrate variability in simulated inherent optical properties for phytoplankton assemblages of changing dominant cell size and functional type. Finally, a preliminary validation is conducted of inherent optical properties determined for natural phytoplankton populations with the two-layered model, using the reflectance approximation. The study demonstrates the validity of the two-layered geometry and refractive index structure, and indicates that the combined use of equivalent size distributions with the heterogeneous geometry can be used to establish a quantitative formulation between single particle optics, size and assemblage-specific inherent optical properties, and ocean colour.

1 Introduction

Understanding the relationship between the dissolved and particulate substances present in the upper ocean, their optical properties, and subsequent effects on the

BGD

6, 1497–1563, 2009

Phytoplankton optical models with two layered spheres

S. Bernard et al.

Title Page

Abstract

Introduction

Conclusions

References

Tables

Figures

◀

▶

◀

▶

Back

Close

Full Screen / Esc

Printer-friendly Version

Interactive Discussion



underwater light field is a principal goal of bio-optical oceanographers. The dominant ecological role of phytoplankton in both oligotrophic and coastal marine systems thus requires that the inherent optical properties of algal populations in natural waters be better understood. Establishing quantifiable relationships between these optical properties and causal cellular characteristics, such as algal size, morphology and intracellular constituent concentrations, is of great importance in the development of bio-optical tools for marine biogeochemical and ecological applications.

The equations of radiative transfer describe the propagation of light through the sea, relating radiative field structure to the inherent optical properties or IOPs (Preisendorfer, 1976). The distribution of radiance within the sea, and the radiance emerging from the sea surface, is thus determined by the spectral nature of the volume scattering and absorption coefficients. Radiative transfer models used for the interpretation and inversion of ocean colour data (Morel and Prieur, 1977; Roesler and Perry, 1995) have parameterised these processes in the form $R \propto b_b / (a + b_b)$, where R is the reflectance, b_b is the backscattering coefficient and a is the absorption coefficient. Understanding the spectral contribution of algal cells to the bulk backscattering coefficient – the integrated angular scattering that is responsible for returning light to the surface of the sea – is thus crucial to ocean colour studies.

Direct spectral measurements of algal backscattering or angular scattering have been rare in the past; the recent availability of angular scattering sensors has done much to improve understanding of the scattering properties of natural and cultured particle and phytoplankton populations (e.g. Chami et al., 2006, 2006a). Mie theory has provided a theoretical alternative to direct measurement, and the current understanding of algal scattering properties is largely based on Mie simulation (Bricaud and Morel, 1986; Ahn et al., 1992; Stramski et al., 2001). However, whilst the absorption, attenuation and total scattering of algal cultures have been successfully simulated using Mie theory (ibid.), and the related anomalous diffraction approximation (ADA) (Van de Hulst, 1957), the few direct measurements made of algal angular scattering suggest that Mie theory is less well suited to describe backward scattering (Quinby-Hunt et al.,

BGD

6, 1497–1563, 2009

Phytoplankton optical models with two layered spheres

S. Bernard et al.

Title Page

Abstract

Introduction

Conclusions

References

Tables

Figures

◀

▶

◀

▶

Back

Close

Full Screen / Esc

Printer-friendly Version

Interactive Discussion



1989; Volten et al. 1998; Vaillancourt et al., 2004; Chami et al., 2006). These studies indicate the importance of internal structure and non-sphericity on algal scattering at large angles; as supported by other studies investigating the effect of internal cellular structure on measured angular scattering (Witkowski et al., 1993, 1998; Svenson et al., 2007); the application of Mie models for algal radiative transfer (Stramski and Piskozub, 2003); and models employing heterogeneous particle geometries (Dunn, 2007).

The extensive use of Mie and ADA modelling in marine bio-optics lies in the relative simplicity of implementation: a spherical geometry with a homogenous refractive index structure can be assumed. It is known that eukaryotic phytoplankton possess heterogeneous intracellular refractive indices, associated with the presence of various membrane systems and intracellular organelles. These include cellular coatings (composed of silicate, cellulose or calcite), membrane bound highly absorbing chloroplasts (containing the chromoprotein complexes necessary for light harvesting and photosynthesis), other membrane bound organelles (such as the mitochondria and nucleus), and regulatory/storage devices (such as gas vacuoles and starch granules). The fact that such internal structures are visible under light microscopy indicates that they are of varying refractive index, and therefore can influence both the internal and external electromagnetic field associated with a cell.

The need to assess the optical impacts of varying internal refractive indices has been addressed by several researchers, with implementations of layered geometry algal optical models. These models have employed either two-layered spheres with the chloroplast as the core (Aas, 1984; Zaneveld and Kitchen, 1995) or three layered spheres with the chloroplast as the central layer (Bricaud et al., 1992; Kitchen and Zaneveld, 1992; Zaneveld and Kitchen, 1995), using volume equivalent refractive index schemes to compare IOPs for homogeneous and heterogeneous spheres. Such studies appear to confirm that backscattering is the IOP most affected by cellular heterogeneity, with heterogeneous geometries resulting in both spectral changes and increases in backscattering magnitude of between 2 and 50. It also appears that adopting a heterogeneous geometry has little effect on absorption and lesser effects on attenuation

**Phytoplankton
optical models with
two layered spheres**S. Bernard et al.

[Title Page](#)[Abstract](#)[Introduction](#)[Conclusions](#)[References](#)[Tables](#)[Figures](#)[Back](#)[Close](#)[Full Screen / Esc](#)[Printer-friendly Version](#)[Interactive Discussion](#)

and total scattering than backscattering – such findings are consistent with the success of homogenous geometry models in simulating algal absorption, attenuation and total scattering (Bricaud and Morel, 1986; Bricaud et al., 1988).

The models described above were used either for small wavelength ranges (Kitchen and Zaneveld, 1992; Zaneveld and Kitchen, 1995), or to investigate the backscattering of coccolithophorids (Bricaud et al., 1992), which can be regarded as exceptional backscatterers in the algal milieu due to their very high refractive index calcite coating.

Such studies demonstrate both the need and the computational ability to produce broadly accessible spectral algal backscattering simulations based on a heterogeneous geometry; a need that is reinforced by the continued emergence of bio-optical techniques and instrumentation for algal and coastal monitoring applications. An improved understanding of the spectral nature of algal backscattering is considered of particular importance, given the well understood effects of anomalous diffraction on angular scattering (Van de Hulst, 1957; Zaneveld and Kitchen, 1995), and the reliance of phylogenetically oriented bio-optical inversion techniques on spectral discrimination (Roesler and Perry, 1995; Garver and Siegel, 1997; Roesler and Boss, 2003).

The numerical and computational capability for heterogeneous cell modelling has existed for several decades (Aden and Kerker, 1951; Meyer, 1979). The relatively sparse implementation of such models regarding algal optics may have resulted at least in part from the paucity of knowledge concerning the optical and morphometrical properties of algal organelles. These difficulties are compounded by the difficulties of translating the highly variable biochemical and structural complexities of eukaryotic cells into an optically or biogeochemically equivalent simple model geometry such as a layered sphere. However, the adoption of a simple layered geometry can allow a simpler perspective a priori: the dependencies of heterogeneous algal optical models can be reduced to the morphometrics of algal ultrastructure, and the determination of suitable effective refractive indices for the primary optical cellular structures. These can be considered to be the chloroplasts as the primary absorbing organelles, the watery cytoplasm typically dominating cell volume, and the external cellular membrane as a high refractive

**Phytoplankton
optical models with
two layered spheres**S. Bernard et al.

[Title Page](#)[Abstract](#)[Introduction](#)[Conclusions](#)[References](#)[Tables](#)[Figures](#)[◀](#)[▶](#)[◀](#)[▶](#)[Back](#)[Close](#)[Full Screen / Esc](#)[Printer-friendly Version](#)[Interactive Discussion](#)

index peripheral layer (Bryant et al., 1969; Aas, 1996; Zaneveld and Kitchen, 1995).

This study will thus seek to investigate the optical properties of algal cells and populations using a two-layered spherical geometry, chosen as the simplest possible heterogeneous structure that has shown itself capable of reproducing measured algal angular scattering properties (Quinby-Hunt et al., 1989). This geometry reduces the effective algal components to a highly absorbing chloroplast containing the protein bound cellular pigments, and a weakly absorbing cytoplasm (Zaneveld and Kitchen, 1995; Stephens 1995). Representative value ranges for relative algal chloroplast volume and complex refractive index will be established, based upon published values. Simple, single cell models will be used to demonstrate the effects of varying cell geometry on optical physiology as given by the package effect (Morel and Bricaud, 1981; Geider and Osborne, 1987), and infer a default cellular geometry. Models assuming this simplified heterogeneous geometry will then be used in conjunction with measured optical and algal size data from natural algal assemblages in the southern Benguela to produce simulated inherent optical properties of typical algal assemblages in an upwelling system.

2 Model theory and structure

2.1 Single particle and wavelength Mie and Aden-Kerker Models

Whilst the details of both Mie (1908) and Aden-Kerker (1951) theory are outside the scope of this study, the implementation of these theories with regard to algal optics can be briefly described as follows (more detail can be found in Morel and Bricaud (1986) or Van de Hulst (1957)). The optical properties of a homogeneous particle interacting with an electromagnetic wave are dependent upon the Mie size parameter α , and complex refractive index m (Morel and Bricaud, 1986). The Mie size parameter is given by:

$$\alpha = \pi d / \lambda_w \quad (1)$$

BGD

6, 1497–1563, 2009

Phytoplankton optical models with two layered spheres

S. Bernard et al.

Title Page

Abstract

Introduction

Conclusions

References

Tables

Figures

◀

▶

◀

▶

Back

Close

Full Screen / Esc

Printer-friendly Version

Interactive Discussion



where d is the particle diameter and λ_w is the wavelength in the surrounding medium – water in this case. The complex refractive index is given by:

$$m = n - n' i \quad (2)$$

where the real part n determines the phase velocity of the propagating wave, and the imaginary part n' determines the flux decay. Note that the effective refractive index is a relative value dependent upon the surrounding medium – all future discussion of refractive index values will assume a relative refractive index in water, with $m_{\text{water}} = 1.334 - 0i$ (Morel and Bricaud, 1986). The effects of employing a two-layered particle geometry are relatively simple: a new size parameter q is introduced describing the core:particle diameter (or radius) where $q = d_{\text{core}}/d$. In addition the refractive indices of both the chloroplast and cytoplasm layers must be explicitly described: the subscripts h for homogeneous, chlor for chloroplast, and cyto for cytoplasm will be used for this purpose where:

$$\begin{aligned} m_h &= n_h - n'_h i && \text{is the refractive index of a homogeneous particle} \\ m_{\text{chlor}} &= n_{\text{chlor}} - n'_{\text{chlor}} i && \text{is the refractive index of the chloroplast layer} \\ m_{\text{cyto}} &= n_{\text{cyto}} - n'_{\text{cyto}} i && \text{is the refractive index of the cytoplasm layer} \end{aligned} \quad (3)$$

The relationship between the imaginary refractive index and the absorption coefficient of the cellular material a_{cm} is useful when considering the effects of intracellular pigment concentration on the refractive index and is given by:

$$n' = a_{\text{cm}} \lambda_w / 4\pi \quad (4)$$

The principal particle optical properties dependent upon these parameters under both Mie and Aden-Kerker theory can be considered to fall into two categories. The optical efficiency factors for absorption Q_a , attenuation, Q_c and scattering Q_b have no angular dependence and can be calculated at relatively little computational cost from complex “Mie coefficients” expressed through spherical Bessel functions (Van de Hulst, 1957; Morel and Bricaud, 1986). The volume absorption a , attenuation c and scattering b

Phytoplankton optical models with two layered spheres

S. Bernard et al.

Title Page

Abstract

Introduction

Conclusions

References

Tables

Figures



Back

Close

Full Screen / Esc

Printer-friendly Version

Interactive Discussion



coefficients can be calculated from these efficiency factors (absorption is used as an example, analogous expressions are used for other coefficients):

$$a = (N/V)sQ_a \quad (5)$$

where N is the number of cells in volume V , and s is the geometrical cross section of the cell.

Optical properties with an angular dependence θ (assuming rotational symmetry) are calculated at greater computational cost and include the volume scattering function (VSF) $\beta(\theta)$, and the phase function $\bar{\beta}(\theta)$ (the scattering normalised VSF), described by:

$$b = 2\pi \int_0^\pi \beta(\theta) \sin \theta d\theta \quad (6)$$

$$\text{and } \bar{\beta}(\theta) = \beta(\theta)/b \quad (7)$$

Integrated scattering parameters in the backward direction include the volume backscattering coefficient b_b , the backscattering probability factor \tilde{b}_b , and the backscattering efficiency factor Q_{bb} described by:

$$b_b = 2\pi \int_{\pi/2}^\pi \beta(\theta) \sin \theta d\theta \quad (8)$$

$$\tilde{b}_b = b_b/b = 2\pi \int_{\pi/2}^\pi \bar{\beta}(\theta) \sin \theta d\theta \quad (9)$$

$$Q_{bb} = \tilde{b}_b Q_b \quad (10)$$

2.2 Size distributions and polydispersions

Algal assemblages are typically polydispersed with regard to size, and can be described by a particle size distribution $F(d)$, where d is the particle diameter, and $F(d)d(d)$ is the number of particles per unit volume in the size range $d \pm 1/2d(d)$.

**Phytoplankton
optical models with
two layered spheres**

S. Bernard et al.

Title Page

Abstract

Introduction

Conclusions

References

Tables

Figures

◀

▶

◀

▶

Back

Close

Full Screen / Esc

Printer-friendly Version

Interactive Discussion



Using absorption as an example (analogous expressions may be used for other coefficients) the absorption efficiency factor representing the mean of a size distribution (as signified by the overbar) can be described as (Morel and Bricaud, 1986):

$$\bar{Q}_a = \frac{\int_0^\infty Q_a F(d) d^2 d(d)}{\int_0^\infty F(d) d^2 d(d)} \quad (11)$$

5 and the resultant volume absorption coefficient is given by either:

$$a = (\pi/4) \int Q_a F(d) d^2 d(d) \quad (12)$$

or, if the result of Eq. (11) is used:

$$a = (\pi/4) \bar{Q}_a \int F(d) d^2 d(d) \quad (13)$$

10 Note that such expressions can be used for the determination of experimental optical efficiency factors, and subsequent refractive index determinations, if measured IOPs and size distributions are known (Bricaud and Morel, 1986; Stramski et al., 1988).

2.3 Anomalous dispersion and spectral refractive indices

15 The above expressions can be applied through a range of wavelengths, and the wavelength dependency λ can be considered implicit in Eqs. (2)–(13). An important consideration in spectral application of particle optical theories is the behaviour of the refractive index in the vicinity of absorption bands. In areas of weak absorption, or low values of the imaginary refractive index, the real refractive index typically decreases with wavelength – termed normal dispersion (Van de Hulst, 1957). However, in the presence of absorption bands, or significant spectral change with wavelength in the imaginary refractive index, the real refractive index increases sharply with wavelength – termed anomalous dispersion (ibid.). This phenomenon can lead to significant spectral variability in the real refractive index and thus considerable spectral shape in the attenuation and various scattering coefficients, typically termed anomalous diffraction.

Title Page

Abstract

Introduction

Conclusions

References

Tables

Figures

◀

▶

◀

▶

Back

Close

Full Screen / Esc

Printer-friendly Version

Interactive Discussion



Phytoplankton optical models with two layered spheres

S. Bernard et al.

Title Page

Abstract

Introduction

Conclusions

References

Tables

Figures

◀

▶

◀

▶

Back

Close

Full Screen / Esc

Printer-friendly Version

Interactive Discussion



The dependence of the real on the imaginary part of the refractive index is described by Ketteler-Helmholtz theory (Van de Hulst, 1957; Bohren and Huffman, 1983), and has often been quantified in application to algal refractive indices using a series of oscillators (representing discrete absorption bands) based on the Lorentz-Lorentz equations (Bricaud and Morel, 1986; Stramski et al., 1988; Zaneveld and Kitchen, 1995). An alternative to the somewhat intricate use of a series of summed Lorentzian oscillators can be found in the Kramers-Kronig relations (Van de Hulst, 1957; Bohren and Huffman, 1983), which allow the spectral variations in the real refractive index to be calculated as a Hilbert transform of the imaginary refractive index. The application of the Kramers-Kronig relations to describing the anomalous dispersion of algal refractive indices has been successfully demonstrated (Bernard et al., 2001; Naqvi et al., 2004). The Kramers-Kronig relations are therefore used here to calculate spectral variations in the real refractive index arising from those in the imaginary refractive index. These follow the notation of Bricaud and Morel (1986), where the spectral variations $\Delta n(\lambda)$ vary around the central part of the real refractive index $1 + \varepsilon$, as given by:

$$n(\lambda) = 1 + \varepsilon + \Delta n(\lambda) \quad (14)$$

2.4 The anomalous diffraction approximation

Somewhat different to the anomalous dispersion effects described above is the anomalous diffraction approximation (ADA), first described by Van de Hulst (1957). The ADA offers approximations to the absorption and attenuation optical efficiency factors using relatively simple algebraic formulae, based on the assumptions that the particle is large relative to wavelength ($a \gg \lambda$) and the refractive index is small ($m - 1 \ll 1$). These important conditions allow the assumption that a ray of light traversing a particle suffers no deflection, and that the attenuation within the particle is thus related simply to path-length. The ADA has been used extensively in algal optics (Bricaud and Morel, 1986; Bricaud et al., 1988; Ahn et al., 1992), partially due to its computational economy, but more importantly because it allows the effects of the real and imaginary refractive

indices on absorption and scattering to be decoupled. This allows the calculation of the imaginary refractive index for algal assemblages, assuming homogeneous geometry and given algal absorption and size distribution data (Bricaud and Morel, 1986; Stramski et al., 1988). The ADA expression for the absorption efficiency factor is given by:

$$Q_a = 1 + \frac{2e^{-\rho'}}{\rho'} + 2\frac{e^{-\rho'} - 1}{\rho'^2}, \quad \rho' = a_{\text{cm}}d = 4an' \quad (15)$$

where ρ' is the absorption optical thickness. Equations (13) and (15) are thus used iteratively in this study to determine homogeneous refractive index data in conjunction with measured algal absorption and particle size distribution data. Whilst it is possible to derive an ADA approximation for two-layered spheres (Quirantes and Bernard, 2004), such a formulation is not used here – all two-layered calculations use the exact Aden-Kerker formulae.

2.5 The package effect

The package effect parameter $Q_a^*(\lambda)$ describes the consequence of placing the absorbing cellular material in particulate as opposed to solution form, and is the ratio of the particulate Chl-*a*-specific absorption $a^*(\lambda)$ to the Chl-*a*-specific absorption of the same material placed perfectly in solution $a_{\text{sol}}^*(\lambda)$. It is given by (Morel and Bricaud, 1981):

$$Q_a^* = \frac{a^*}{a_{\text{sol}}^*} \quad (16)$$

$$Q_a^* = \frac{3}{2} \frac{Q_a}{a_{\text{cm}}d} \quad (17)$$

An additional relationship can be described which introduces the intracellular Chl-*a* concentration c_j (kg m^{-3}):

$$a_{\text{sol}}^* = \frac{a_{\text{cm}}}{c_j} \quad (18)$$

Phytoplankton optical models with two layered spheres

S. Bernard et al.

Title Page

Abstract

Introduction

Conclusions

References

Tables

Figures

◀

▶

◀

▶

Back

Close

Full Screen / Esc

Printer-friendly Version

Interactive Discussion



Phytoplankton optical models with two layered spheres

S. Bernard et al.

Title Page

Abstract

Introduction

Conclusions

References

Tables

Figures

◀

▶

◀

▶

Back

Close

Full Screen / Esc

Printer-friendly Version

Interactive Discussion



It should be noted that Eq. (17) is an exact derivation, and is not limited (from a strict theoretical perspective) by the same assumptions as the ADA with regard to size and refractive index. This will obviously not hold true if the Q_a term in Eq. (17) is calculated with the ADA as opposed to an exact solution (Latimer, 1984; Geider and Osborne, 1987). Cellular packaging has important physiological consequences, as it will impact upon the ability of a cell to make incident energy available for photosynthesis (Raven, 1984; Finkel and Irwin, 2000), and the ability of a cell to dissipate energy through fluorescence (Babin et al., 1996). The effect of varying cellular geometry on the package effect is considered here, and an expression for the package effect of a two-layered sphere, based on Gladstone-Dale volume equivalence (Aas, 1996), is derived as:

$$Q_a^* = \frac{3}{2} \frac{Q_a}{\left(a_{\text{cm}}^{\text{core}} q^3 + a_{\text{cm}}^{\text{shell}} [1 - q^3] \right) d} \quad (19)$$

where Q_a is the absorption efficiency factor of the two layered sphere (dimensionless), $a_{\text{cm}}^{\text{core}}$ is the absorption of cellular material for the particle core (m^{-1}), $a_{\text{cm}}^{\text{shell}}$ is the absorption of cellular material for the particle shell (m^{-1}), and q is the ratio of the core: shell radii (dimensionless). The above expression is obviously dependent upon the validity of the volume equivalence term for the effective optical thickness, and it can be tested against a direct calculation of the package effect, as follows. If the imaginary refractive indices of a hypothetical two-layered particle population are known, the a_{cm} values for both layers can be calculated from Eq. (4). The hypothetical total absorption in solution can be calculated as:

$$a_{\text{sol}} = \frac{\pi}{6} \int F(d) d^3 d(d) \left(a_{\text{cm}}^{\text{core}} q^3 + a_{\text{cm}}^{\text{shell}} (1 - q^3) \right) \quad (20)$$

Assuming the particulate absorption is known from model output, the package effect parameter can then be calculated with Eq. (16).

All optical modelling in this study for both heterogeneous and homogeneous particles, apart from package effect calculations as discussed above, were made with the

two-layered code of Toon and Ackerman (1981) with size bins of 1 μm and an angular resolution of 0.1°. The suitability of the Toon and Ackerman code for homogeneous modelling was verified by comparison with the Bohren and Huffman (1983) code – identical results were found across a wide variety of size and refractive indices. All models were run under a combined Matlab R13 (The Mathworks) and Fortran (Compaq Visual Fortran V6.5) environment.

3 Morphometrics and refractive indices of the algal cell

3.1 Chloroplast morphometrics

The chloroplast of an autotrophic eukaryotic cell is the membrane bound organelle containing the highly absorbing pigment-protein complexes responsible for light harvesting and photosynthesis, and it will exert a profound optical effect. Algal related studies investigating the effects of cellular internal structure on scattering (Witkowski et al., 1993, 1998) and absorption packaging (Geider and Osborne, 1987) indicate the importance of chloroplasts in modifying both the absorbing and scattering properties of algal cells.

Imposing a simple two-layered geometry upon a hypothetical algal cell thus requires some knowledge of the variability of chloroplast size, or more appropriately, the relative chloroplast volume. Phytoplankton cells exhibit wide variability with regard to chloroplast morphology: the total number of chloroplasts is highly variable, and they exhibit a wide variety of shapes, size and membrane structure. Physiology is also known to strongly influence cell structure: photoadaptation, temperature, life stage, nutrient and trace element history can all influence chloroplast volume, location, internal structure and internal pigment density (Jeffrey and Vesk, 1977; Thinh 1983, Rosen and Lowe, 1984).

Table 1 details relative chloroplast volumes V_v derived from published data for a range of cultured algal species, which show V_v values ranging from 4.4 to 57% (cf. 3 to 66% from Geider and Osborne, 1987). There appears no significant rela-

BGD

6, 1497–1563, 2009

Phytoplankton optical models with two layered spheres

S. Bernard et al.

Title Page

Abstract

Introduction

Conclusions

References

Tables

Figures

◀

▶

◀

▶

Back

Close

Full Screen / Esc

Printer-friendly Version

Interactive Discussion



tionship between cell size, as given by the equivalent volume spherical diameter, and chloroplast volume – this may be a function of the small data set in Table 1 (published morphometric chloroplast data is scarce) which incorporates a wide range of growth conditions and species.

5 Nevertheless, within the context of this study, it is reasonable to assume a size-independent relative chloroplast volume of 20% (the median value from Table 1) as a first approximation for a spherical algal geometry. The use of a size invariant V_v value can be justified by evidence suggesting that the algal protein to Chl-*a* ratio is relatively invariant to changing cell size, and thus the proportion of cytoplasmic mass devoted to chloroplasts is independent of size (Hitchcock, 1982; Moal et al., 1987; 10 Montagnes et al., 1994). To aid visualisation in comparison to a typical transmittance electron micrograph, a V_v value of 20% would result in an inner relative radius q of 0.58 if the inner layer of a two-layered sphere is considered the chloroplast. Previous modelling studies employing heterogeneous geometries with dedicated chloroplast layers have employed relative chloroplast volumes of $V_v=41\%$ (Zaneveld and Kitchen, 15 1995), $V_v=58\%$ (Latimer, 1984), and $V_v=27\%$ to 66% (Bricaud et al., 1992). These are in all cases considerably higher than the preliminary V_v value assumed here, and fall amongst the higher values reported in Table 1. Nevertheless, a V_v value of 20% for a dedicated chloroplast layer is considered appropriate given the available morphometric data. Additionally, the primary focus of this study is ocean colour related 20 applications, and thus high-light adapted algae from the upper optical depths. The assumption of a relatively small chloroplast volume is consistent with observations of smaller chloroplast volume in high-light adapted cells, as shown in Table 1.

3.2 Real part of the algal refractive index

25 The real refractive index of a homogeneous algal cell is the primary causal variable with regard to the magnitude of algal scattering (Morel and Bricaud, 1986). Whilst the same is true as concerns a cell of heterogeneous geometry, complexities are introduced by the presence of additional refractive index boundaries corresponding to simulated

**Phytoplankton
optical models with
two layered spheres**

S. Bernard et al.

Title Page

Abstract

Introduction

Conclusions

References

Tables

Figures



Back

Close

Full Screen / Esc

Printer-friendly Version

Interactive Discussion



internal structures (Meyer, 1979; Zaneveld and Kitchen, 1995).

The assumption of a two-layered geometry gives critical importance to the establishment of suitable chloroplast refractive index ranges. It should be realised that chloroplasts are far from homogeneous, and the adoption of a single refractive index value or spectra is itself a simplification. The chloroplast is enclosed in two to four outer membranes, and consists of stacked thylakoid membranes containing the pigment-protein complexes, embedded within the stroma. Thylakoid stacking and areal chlorophyll density is variable (Rosen and Lowe, 1984; Berner et al., 1989), and the thylakoid membranes can exhibit considerable birefringence (Paillotin et al., 1998). Changes in membrane stacking and transparency can affect light absorption due to an intracellular package effect (Jennings and Zucchelli, 1985; Berner et al., 1989). However, accounting for phenomena arising from chloroplast heterogeneity is beyond the scope of this study, and the chloroplast will necessarily be considered homogeneous here.

Table 2 provides considerable evidence that the real refractive index of chloroplasts, or the material contained therein, are considerably higher than values published for homogeneous cells. The chloroplast related data, from a wide range of sources, display central real refractive index $1+\varepsilon$ values of between 1.06 to 1.22 (excluding highest and lowest values as extrema), as compared to homogeneous cell values of 1.01 to 1.09 (Bricaud et al. 1988, Ahn et al., 1992). However, taking chloroplast $1+\varepsilon$ values of 1.06 to 1.22, a cytoplasm $1+\varepsilon$ value of 1.02, and a relative chloroplast volume of 20%, the homogeneous volume equivalent $1+\varepsilon$ values under the Gladstone-Dale scheme range from 1.028 to 1.060 – consistent with experimentally determined homogeneous values (ibid.). Whilst simple volume equivalent or effective medium schemes are approximate from an optical perspective (Chylek and Videen, 1998), this consistency indicates that the chloroplast volume and real refractive index ranges suggested by Tables 1 and 2 are entirely appropriate from both an optical and cellular composition perspective. For preliminary analyses, a chloroplast $1+\varepsilon$ value of 1.14 will be used, as the extrema rejected mean from Table 2.

Few measurements of cytoplasm refractive indices have been published – Table 2

BGD

6, 1497–1563, 2009

Phytoplankton optical models with two layered spheres

S. Bernard et al.

Title Page

Abstract

Introduction

Conclusions

References

Tables

Figures

◀

▶

◀

▶

Back

Close

Full Screen / Esc

Printer-friendly Version

Interactive Discussion



shows the single value of $1+\varepsilon=1.015$ (Charney and Brackett, 1961). Previous studies have adopted either this value (Bricaud et al., 1992) or similar values of 1.02 (Kitchen and Zaneveld, 1992; Zaneveld and Kitchen, 1995). Variations in the algal real refractive index are typically considered as due to changes in the relative amounts of cellular water and solids, rather than changes in the chemical composition of solids (Aas, 1996; Stramski, 1999). The low reported refractive index values for cytoplasm are thus consistent with an expectedly high water content (Aas, 1996). A value of $1+\varepsilon=1.02$ for cytoplasm will be adopted for this study.

3.3 Imaginary part of the algal refractive index

A useful conceptual framework in algal optics is to consider that unpackaged Chl-*a*-specific absorption has theoretical maxima, based on either absorption measurements of Chl-*a* in solvent, or of isolated chromoproteins (Bricaud et al., 1995; Johnsen et al., 1994). Based on this construct, the unpackaged Chl-*a*-specific absorption can be normalised to a theoretical maximum at ~ 675 nm – the wavelength of the red Chl-*a* absorption peak where Chl-*a* is considered the sole absorber (ibid.). Under a two-layered geometry, it is possible to combine Eqs. (4), (18) and the Gladstone-Dale expression of volume equivalence to allow the calculation of the imaginary refractive index of the chloroplast layer at 675 nm:

$$n'_{\text{chlor}}(675) = \frac{675}{n_{\text{media}}} \frac{\pi c_l a_{\text{sol}}^*(675)}{4V\nu} \quad (21)$$

where $n_{\text{media}}=1.334$ and $V\nu$ is the relative chloroplast volume. Equation (21) thus describes the relationship between the intracellular Chl-*a* concentration, chloroplast volume, chloroplast imaginary refractive index, and cellular absorption, based on the assumption that the cytoplasm layer has no significant absorption at 675 nm.

Equation (21) offers a useful starting point to examine the potential range and behaviour of the imaginary refractive index for algal chloroplasts n'_{chlor} , or more accurately the simulated chloroplast layer in a hypothetical two-layered geometry. It can

Phytoplankton optical models with two layered spheres

S. Bernard et al.

Title Page

Abstract

Introduction

Conclusions

References

Tables

Figures

◀

▶

◀

▶

Back

Close

Full Screen / Esc

Printer-friendly Version

Interactive Discussion



be seen that n'_{chlor} is dependent upon the relative chloroplast volume and the intracellular Chl-*a* concentration c_i , based on Gladstone-Dale volume equivalence. Whilst it would be more desirable to employ chloroplast (as opposed to intracellular) Chl-*a* concentrations, and thus dispense with the need for a volume equivalence scheme, such chloroplast data are very rare (unknown to the authors). The dependence of n'_{chlor} upon c_i is therefore considered a necessary approximation, and at least allows consideration of algal optical properties armed with a considerable body of published c_i data (e.g. Taguchi, 1976; Malone, 1980; Bricaud et al., 1988). In addition, published relationships between c_i and $n'_h(675)$ for homogeneous cells (Stramski, 1999; Eq. 9) can be used for comparative purposes. A reasonable range of algal c_i values could be considered 0.5 to 10 kg m⁻³ (Taguchi, 1976; Malone, 1980; Bricaud et al., 1988) – these would produce homogenous $n'_h(675)$ values of ~0.0005 to 0.011, using Eq. (18) and $a_{\text{sol}}^*(675)=0.027 \text{ mg}^{-1} \text{ m}^{-2}$ (Johnsen, 1994), or values of 0.0017 to 0.011 using the Stramski formulation. These data ranges compare well with published values (Ahn et al., 1992; Stramski et al., 2001), and confirm the use of the Stramski formula as a validation check. The equivalent chloroplast $n'_{\text{chlor}}(675)$ value range using Eq. (21) with $V_V=20\%$ is ~0.0027 to 0.054, as compared to a range from the Stramski formula of ~0.0037 to 0.051. Whilst the Stramski formula is designed for use with homogeneous cells as opposed to chloroplasts, the close comparison of the two $n'_{\text{chlor}}(675)$ data ranges (from Eq. 21 and the Stramski formula) is encouraging, given their derivation from very different sources. Previous heterogeneous modelling studies have employed n'_{chlor} values of 0.024 in the 670 nm region (Zaneveld and Kitchen, 1995) or 0.04 to 0.05 at 442 nm (Quinby-Hunt et al., 1989), which fall within the proposed range of values from Eq. (21).

The spectral shape of the cellular imaginary refractive indices will be discussed in detail later, in relation to the application of inverse refractive index models to measured algal optical data. Briefly, the spectral imaginary refractive index of the chloroplast layer can be estimated to a first order using volume equivalence, if homogeneous and cytoplasm data are known or assumed. Few imaginary refractive index data are available

**Phytoplankton
optical models with
two layered spheres**

S. Bernard et al.

Title Page

Abstract

Introduction

Conclusions

References

Tables

Figures

◀

▶

◀

▶

Back

Close

Full Screen / Esc

Printer-friendly Version

Interactive Discussion



for cellular cytoplasm. However, it would appear that the cytoplasm is weakly absorbing, with an exponential type spectral shape typical of non-pigmented organic compounds (Stephens, 1995). The cytoplasm imaginary refractive index is thus expected to be small but significant at blue wavelengths, decreasing to insignificant values in the red.

For preliminary single particle analyses to investigate the broad characteristics of a two-layered geometry, an n'_{chlor} value of 0.02 and an n'_{cyto} value of 0.0005 will be used, considered typical values in the Soret spectral region, e.g. 435 nm. Detailed spectral data for the imaginary refractive indices will be revisited later.

3.4 Cellular morphometrics

Having established reasonable morphometric and refractive index data ranges, it is necessary to assess the assignment of the two layers available – is it more appropriate from a general perspective to model the chloroplast as the inner or outer layer? It must be appreciated that such a synthetic construct is a vast oversimplification – chloroplast phototaxis is a known phenomena (Rosen and Lowe, 1984; Stephens, 1995) and the variability of chloroplast morphometrics has been discussed previously. Nevertheless, a simplified cell geometry can be mathematically simulated, and to this end the implications of selecting a central or peripheral chloroplast layer can be assessed.

Figure 1 shows the optical efficiency factors and backscattering probability of particles using the geometrical and refractive index values discussed above, for a range of Mie size values. The α values used are compatible with a particle diameter range of 1 to 96 μm and a wavelength of 435 nm. The efficiency factors of interest to this discussion are the absorption efficiency factor Q_a and the package effect parameter Q_a^* . Figure 1e demonstrates the considerable difference in packaging between the inner and outer chloroplast models – the inner model has Q_a^* values approximately up to 40% lower (meaning that the absorption packaging is approximately 40% higher). In comparison, the packaging of the homogeneous and outer layer model differ by a maximum of 10%. Figure 1c reveals that it is the difference in Q_a values that is the

Title Page

Abstract

Introduction

Conclusions

References

Tables

Figures



Back

Close

Full Screen / Esc

Printer-friendly Version

Interactive Discussion



predominant cause of these packaging differences. The inner chloroplast model has considerably lower absorption efficiency factors, particularly so at larger sizes where it tends toward a lower limiting value than the theoretical maximum of one (Morel and Bricaud, 1986).

5 The outer chloroplast model appears to be a more appropriate choice for general application for several reasons. It can be assumed, from a general phyiological cost-benefit perspective, that an algal cell will benefit from minimising absorption packaging (Raven, 1984). Direct measurements of absorption packaging indicate that packaging tends to be lower than predicted by theory, i.e. Q_a^* is closer to one (Geider and Osborne, 10 1987; Osborne and Geider, 1989). Given both these factors, it would thus seem reasonable to adopt a model geometry that minimises packaging – the outer chloroplast model. Previous studies have also suggested that a high refractive index peripheral layer is beneficial to a cell in terms of light trapping (Latimer, 1984; Geider and Osborne, 1987; Zaneveld and Kitchen, 1995). In addition, the inner chloroplast model 15 typically yields Q_a values smaller than ~ 0.5 , except for very large cell sizes of $>30\ \mu\text{m}$ diameter. Reported experimental Q_a values considerably larger than 0.5 are not uncommon (Iturriaga and Sigel, 1989; Ahn et al., 1992; Stephens, 1995), and the inability of the inner chloroplast model to simulate large Q_a values at typical algal diameters of $<30\ \mu\text{m}$ diameter indicates that this geometry may be less suitable.

20 A further reason for adopting an outer chloroplast model geometry lies in the restrictions of a two-layered geometry – this precludes the specific assignation of a high refractive index external membrane or coating, structures shown to have considerable impact on backscattering (Meyer, 1979; Bricaud et al., 1992; Zaneveld and Kitchen, 1995). Table 2 indicates similar real refractive index values of ~ 1.12 – 1.14 for chloroplasts and the various forms of external membrane or coating material (excluding the 25 calcite coatings of coccolithophores which must be considered a special case). The intracellular refractive index gradient of the outer layer model will therefore be most similar to a hypothetical three layered model with an explicit peripheral membrane layer. In effect, the three layered model would simply have a thin peripheral layer outside the

BGD

6, 1497–1563, 2009

Phytoplankton optical models with two layered spheres

S. Bernard et al.

Title Page

Abstract

Introduction

Conclusions

References

Tables

Figures

◀

▶

◀

▶

Back

Close

Full Screen / Esc

Printer-friendly Version

Interactive Discussion



central chloroplast layer, of similar real refractive index and zero imaginary refractive index (Zaneveld and Kitchen, 1995). Differences in the scattering behaviour of the outer chloroplast two layer model and a hypothetical three layer model can reasonably be expected to be small, particularly in comparison to an inner chloroplast two layer model.

Examination of transmittance electron micrographs from morphometrical studies confirm that, for a wide variety of species, chloroplasts are located peripherally. These include a range of diatom species (Hoops and Floyd, 1979; Sicko-Goad and Stoermer, 1979; Hitchcock, 1982; Rosen and Lowe, 1984; Janssen et al., 2001), dinoflagellates with single (Highfill and Pfiester, 1992; Jenks and Gibbs, 2000) and many radial chloroplasts (Messer and Ben-Shaul, 1972; Dodge and Crawford, 1969; Spector and Triemer, 1979), pelagophytes (Gastrich et al., 1998; Pitcher et al., 1999), chlorophytes (Rosen et al., 1986), eustigmophytes (Fisher et al., 1998), and cryptophytes (Thin, 1983). An outer chloroplast geometry will therefore be adopted for the remainder of this study.

4 Comparative geometry and causal variability

Figure 1a and b shows the typical oscillating behaviour with changing α of the attenuation and scattering efficiency factors (Van de Hulst, 1957; Morel and Bricaud, 1986). Similar behaviour was noted by Aas (1984), and it can be seen that the outer layer model causes greater amplitude oscillations in both Q_c and Q_b , whilst tending to the same approximately constant values of $Q_c=2$ and $Q_b=1$ at large sizes (Morel and Bricaud, 1986). The behaviour of the Q_a values in Fig. 1c have been discussed above – the behaviour displayed is again consistent with previous results (Morel and Bricaud, 1981), in that the homogeneous and outer layer model produce similar results (Aas, 1984). The largest differences arising from heterogeneity can be seen in the enhanced backscattering efficiency Q_{bb} (Fig. 1d) and backscattering probability \tilde{b}_b (Fig. 1f) values associated with the outer layer model. The Q_{bb} values of the outer layer model are between 5 and 25 times higher than the homogeneous model, converging

Phytoplankton optical models with two layered spheres

S. Bernard et al.

Title Page

Abstract

Introduction

Conclusions

References

Tables

Figures

◀

▶

◀

▶

Back

Close

Full Screen / Esc

Printer-friendly Version

Interactive Discussion



to an approximately constant value at high sizes of $Q_{bb} \approx 0.0025$ – 9 times higher than the homogeneous model. Roughly the same comparisons hold for the backscattering probability factor values. It can be seen in both cases (Fig. 1d and f) that the somewhat chaotic structure in the backscattering vs size relationships (Morel and Bricaud, 1986) is also appreciably different for the contrasting model geometries.

The effects of varying chloroplast size can be seen with regard to comparison of heterogeneous cells of varying volume equivalence relative to homogeneous cells with a constant refractive index (Fig. 2). Changes in chloroplast size whilst maintaining volume equivalence have only small effects on attenuation, scattering, absorption and the package effect parameter (Fig. 2a–c, and e). The converse appears to be true with regard to backscattering parameters from heterogeneous cells. Backscattering efficiency and probability factors of the heterogeneous volume equivalent cells (Fig. 2d and f) show considerable variability with changing chloroplast size and refractive index. Values of heterogeneous Q_{bb} and \tilde{b}_b range from approximately 2 to 35 times higher than homogeneous values, with considerable dependence on α ; somewhat chaotic at $\alpha < 400$ and approximately constant thereafter. The approximately constant Q_{bb} values at high sizes ($\alpha > 400$) can be used as a convenient comparison: these are 0.004 ($V_v = 15\%$, $n_{\text{chlor}} = 1.18$), 0.0025 ($V_v = 20\%$, $n_{\text{chlor}} = 1.14$), 0.0014 ($V_v = 30\%$, $n_{\text{chlor}} = 1.10$), and 0.00028 (homogeneous, $n = 1.044$). These comparisons reveal not only that heterogeneous cells backscatter considerably more than their homogeneous equivalents, but behave in very different ways in response to refractive index changes. It would appear that the real refractive index of the outer chloroplast layer (or any peripheral layer) could be considered the single most important intracellular causal variable for backscattering; certainly more important than the relative size of the peripheral layer. Such conclusions are at least partially supported by previous heterogeneous modelling studies (Meyer, 1979; Zaneveld and Kitchen, 1995).

The effects of variations solely in the imaginative refractive index are shown in Fig. 3, where the value of n'_{chlor} is varied from 0.001 to 0.04. Resultant variations for Q_c (Fig. 3a) and Q_b (Fig. 3b) are consistent with the data of Morel and Bricaud (1986) –

**Phytoplankton
optical models with
two layered spheres**

S. Bernard et al.

Title Page

Abstract

Introduction

Conclusions

References

Tables

Figures

◀

▶

◀

▶

Back

Close

Full Screen / Esc

Printer-friendly Version

Interactive Discussion



increases in the imaginary refractive index, responsible for absorption, result in damping of the typical oscillation patterns in these variables. Damping effects are observed for both homogeneous and heterogeneous geometries, although they appear more pronounced for the latter – perhaps due to the higher n'_{chlor} values relative to the homogeneous volume equivalent n'_h values. Geometry related effects on absorption (Fig. 3c) and the package effect parameter (Fig. 3e) are not pronounced for volume equivalent cells with a maximum difference of $\sim 12\%$. Again, the general increase in Q_a and decrease in Q_a^* with increasing n'_{chlor} are consistent with previous observations (Morel and Bricaud, 1981; 1986).

Backscattering parameters for heterogeneous geometries appear to be affected in similar ways to total scattering – α related oscillations are more heavily dampened with increasing n'_{chlor} and become approximately constant at high α ($Q_{bb}=0.0025$ to 0.0027). Homogeneous backscattering with increasing α displays a different structure; a pronounced backscattering maxima at $\alpha \approx 200$ to 300 , which disappears with increasing n'_h values – a phenomenon that has been observed previously (Morel and Bricaud, 1986). Of particular importance are the considerably elevated backscattering values at very low imaginary refractive index values; the potential effects of this will be discussed later with regard to spectral backscattering characteristics.

The effects of variations in polydispersity can be seen in Fig. 4, displaying data for single sizes and Standard distributions (Hansen and Travis, 1974) of differing effective variance (or width). The Q_c (Fig. 4a) and Q_b (Fig. 4b) data are consistent with the finding of Morel and Bricaud (1986) – increased polydispersion results in greater damping of the oscillation patterns in these variables, leaving only the first oscillation peak at $\alpha \approx 60$ still prominent. Absorption would appear to be affected primarily by the inclusion of smaller sizes as polydispersion increases, with Q_a values at $v_{\text{eff}}=0.6$ up to 15% lower than the monodispersed values (Fig. 4c) – package effect parameter values are consistent with this (Fig. 4e). Geometry related variability remains small, with maximal 10% differences between homogeneous and heterogeneous absorption. The effects of polydispersity on backscattering are consistent with previous studies (Morel

**Phytoplankton
optical models with
two layered spheres**S. Bernard et al.

[Title Page](#)[Abstract](#)[Introduction](#)[Conclusions](#)[References](#)[Tables](#)[Figures](#)[◀](#)[▶](#)[◀](#)[▶](#)[Back](#)[Close](#)[Full Screen / Esc](#)[Printer-friendly Version](#)[Interactive Discussion](#)

and Bricaud, 1986) – the finer scale chaotic behaviour in both Q_{bb} (Fig. 4d) and \tilde{b}_b (Fig. 4f) are smoothed. Increased polydispersity leads to slightly higher backscattering values at large sizes due to the greater inclusion of smaller particles in the size distribution. It can also be seen that very low imaginary refractive index values lead to profound changes in selected optical properties – these will be discussed later with regard to the spectral nature of modelled inherent optical properties.

5 Comparative geometry and spectral inherent optical properties

5.1 Determination of refractive indices for algal populations

Modelling the full spectral inherent optical properties of an algal population requires the derivation of the refractive index spectra; either $m_h(\lambda)$ for homogeneous cells, or $m_{\text{chlor}}(\lambda)$ and $m_{\text{cyto}}(\lambda)$ for two-layered cells. Measurements of phytoplankton absorption and size distributions allow the calculation of experimental absorption efficiency factors using Eq. (13) (Bricaud and Morel, 1986; Stramski et al., 1988). From these data the imaginary refractive index, and the spectral shape of the real refractive index, can be determined (as discussed previously) for both homogeneous cells and the layers of heterogeneous cells. The real refractive index spectra $n(\lambda)$, of either the homogeneous cell or its constituent layers, can then be calculated using Eq. (14), through the selection of appropriate $1+\varepsilon$ values.

It is possible to make direct determinations of $1+\varepsilon$ values for homogeneous cells through the ADA – this would require additional use of attenuation or scattering data, not available to this study (Bricaud and Morel, 1986; Stramski et al., 1988). Even if such data were available, it would be extremely difficult to determine real and imaginary refractive index spectra for both chloroplast and cytoplasm from optical and size measurements. The ADA, allowing the decoupling of the real and imaginary refractive index, is typically used for such purposes as an iterative inverse efficiency factor model for homogeneous cells (ibid.). Whilst an ADA formulation is available for a two-layered

Title Page

Abstract

Introduction

Conclusions

References

Tables

Figures

◀

▶

◀

▶

Back

Close

Full Screen / Esc

Printer-friendly Version

Interactive Discussion



Phytoplankton optical models with two layered spheres

S. Bernard et al.

Title Page

Abstract

Introduction

Conclusions

References

Tables

Figures

◀

▶

◀

▶

Back

Close

Full Screen / Esc

Printer-friendly Version

Interactive Discussion



geometry (Quirantes and Bernard, 2004), it is unlikely to satisfy the original ADA assumption that the real refractive index is small ($m-1 \ll 1$) (Van de Hulst, 1957), given the high chloroplast refractive indices suggested by Table 2. Two-layered application of the iterative modelling approach to refractive index determination of Stramski et al. (1988) would thus require invocation of the full Aden-Kerker formulae, dealing with the four unknowns of real and imaginary refractive index for both layers. Such a model was constructed and applied to sample data from Bricaud et al. (1988). The results (not presented here) indicate that multiple solutions abound even with very close matches for absorption and attenuation data, i.e. a priori assumptions concerning the spectral refractive indices of layers must be made to return feasible model solutions. The dependence of the study upon $1+\varepsilon$ values gleaned from the literature, most specifically for simulated chloroplasts, is thus not inappropriate.

Preliminary two-layered modelling efforts also indicated the need for assumed refractive index values of the cytoplasm. Based on the intracellular optical efficiency measurements of Stephens (1995), the typical exponential spectral shape of organic detrital particles (Itturiaga and Siegel, 1989), and trial modelling runs, the imaginary refractive index for cytoplasm was chosen to be:

$$n'_{\text{cyto}}(\lambda) = n'_{\text{cyto}}(400) \exp[-0.01(\lambda - 400)] \quad (22)$$

where $n'_{\text{cyto}}(400) = 0.0005$. Real refractive index spectra for the cytoplasm $n_{\text{cyto}}(\lambda)$ were then generated with a Hilbert transform under Matlab R13 (The MathWorks), and Eq. (14) with $1+\varepsilon = 1.02$.

Given such considerations, refractive index spectra for sample natural algal populations have therefore been determined in three different ways. To generate initial values for homogeneous cells, $n'_h(\lambda)$ spectra were calculated using Eq. (15) (Stramski et al., 1988). Using the $n'_{\text{cyto}}(\lambda)$ values of Eq. (22), volume equivalent $n'_{\text{chlor}}(\lambda)$ values were determined using the Gladstone-Dale formulation given by:

$$n'_{\text{chlor}}(\lambda) = (n'_h(\lambda) - n'_{\text{cyto}}(\lambda)Vv)/(1 - Vv) \quad (23)$$

where V_V is the chloroplast volume. Real refractive index spectra for the chloroplast $n_{\text{chlor}}(\lambda)$ were then similarly generated with a Hilbert transform, and Eq. (14) with assumed $1+\varepsilon$ values as discussed below.

In addition to the volume equivalent generation of $n'_{\text{chlor}}(\lambda)$, a further method based on direct application of the Aden-Kerker formulae was employed, designed to provide greater accuracy of refractive index determination. Using the volume equivalent m_{chlor} and m_{cyto} values just described as initial input, a non-linear solution of Eq. (11) was implemented, employing a simplex routine (Nelder and Mead, 1965) and the Toon and Ackerman (1981) code. Solving for experimental Q_a values with measured size distributions, the model was allowed several passes through the entire wavelength range to yield $n'_{\text{chlor}}(\lambda)$ and $n_{\text{chlor}}(\lambda)$ values consistent with Aden-Kerker theory and the Kramers-Kronig relations, with $m_{\text{cyto}}(\lambda)$ held constant.

Sample absorption and size distribution data from natural algal assemblages in the southern Benguela are used as input to the refractive index models. Briefly, particulate and detrital absorption data were measured with the quantitative filter pad technique (Yentsch, 1962; Roesler, 1998; Kishino et al., 1985) using a Shimadzu UV-2501 spectrophotometer equipped with an ISR-2200 internal integrating sphere. Phytoplankton absorption $a_\phi(\lambda)$ data were then obtained by subtraction of detrital absorption $a_d(\lambda)$ from total particulate absorption $a_p(\lambda)$. Particle size measurements were made using a 128 channel Coulter Multisizer II with a 140 μm aperture in manometer mode, using freshly prepared 0.2 μm filtered seawater as both blank and electrolyte. Numerical techniques (Bernard et al., 2007) were employed to fractionate measured size distributions into algal and non-algal components, and extend both lower and upper ranges of measured size distributions to match absorption measurements. Pigments were analysed using High Performance Liquid Chromatography (HPLC) using the methods of (Barlow et al., 1997). Detailed methods for all measurements are presented in Bernard et al. 2007.

Four assemblages types common to upwelling systems (Hutchings et al., 1994) were chosen for detailed analysis. These are: an offshore assemblage

**Phytoplankton
optical models with
two layered spheres**S. Bernard et al.

[Title Page](#)[Abstract](#)[Introduction](#)[Conclusions](#)[References](#)[Tables](#)[Figures](#)[◀](#)[▶](#)[◀](#)[▶](#)[Back](#)[Close](#)[Full Screen / Esc](#)[Printer-friendly Version](#)[Interactive Discussion](#)

Phytoplankton optical models with two layered spheres

S. Bernard et al.

Title Page

Abstract

Introduction

Conclusions

References

Tables

Figures

◀

▶

◀

▶

Back

Close

Full Screen / Esc

Printer-friendly Version

Interactive Discussion



dominated by small Chlorophytes and Prymnesiophytes (flagellate, $d_{\text{eff}}=4.3\ \mu\text{m}$, $\text{Chl-}a=0.59\ \text{mg m}^{-3}$, $c_i=1.5\ \text{kg m}^{-3}$), a diatom dominated assemblage (diatom, $d_{\text{eff}}=8.3\ \mu\text{m}$, $\text{Chl-}a=6.1\ \text{mg m}^{-3}$, $c_i=2.3\ \text{kg m}^{-3}$), an assemblage dominated by the dinoflagellates *Alexandrium catenella* and *Ceratium* spp. (dinoflagellate, $d_{\text{eff}}=26\ \mu\text{m}$, $\text{Chl-}a=126\ \text{mg m}^{-3}$, $c_i=4.0\ \text{kg m}^{-3}$), and a mixed assemblage of diatoms and the Cryptophyte endosymbiont containing ciliate *Mesodinium rubrum* (cryptophyte, $d_{\text{eff}}=14\ \mu\text{m}$, $\text{Chl-}a=195\ \text{mg m}^{-3}$, $c_i=3.1\ \text{kg m}^{-3}$). Dominant accessory pigments for these samples are: chlorophyll *c*-chlorophyll *b*-fucoxanthin derivatives (flagellate), chlorophyll *c*-fucoxanthin-diadinoxanthin (diatom), chlorophyll *c* – peridinin-diadinoxanthin (dinoflagellate), and chlorophyll *c* – alloxanthin (cryptophyte).

The measured and derived refractive index data for the four example assemblages are shown in Fig. 5. Measured *Chl-}a*-specific phytoplankton absorption (Fig. 5a) show the effects of size-related packaging, most obvious when comparing the flagellate and dinoflagellate samples, dominated by small and large cells respectively. The effects of differences in accessory pigment complements can also be seen, most prominently in the phycoerythrin affected cryptophyte sample (Gustafson et al., 2000). *Chl-}a*-normalised volume size distributions (Fig. 5b) show the typically highly polydispersed nature of natural algal assemblages, even in high biomass bloom situations, particularly so for the cryptophyte sample, which is composed of small celled diatoms and the large celled *Mesodinium rubrum*.

Modelled absorption efficiency factor data used for the direct two-layered refractive index determinations show a very close match (Fig. 5c) to experimentally determined Q_a values, indicating the successful simulation of the heterogeneous model. It should be noted that the two-layered refractive index model utilising the Aden-Kerker code was unable to produce appropriately smooth n'_{chlor} values when using the default V/v value of 20% for the large celled dinoflagellate and cryptophyte samples. Appropriately shaped n'_{chlor} spectra (i.e. those without significant spikes) were only obtained when minimal V/v values of 30% were adopted for these two samples. It would appear that this is due to the high experimental Q_a values for these samples (Fig. 5c), and the

relatively higher Q_a values theoretically possible when higher Vv values are adopted (Figs. 2c and 3c). Relatively high Q_a values are associated with high values of either of the two variables causal to absorption – cell diameter d_{eff} or intracellular Chl-*a* concentration c_i (Morel and Bricaud, 1981; Bricaud et al. 1988, Ahn et al., 1992). Consistent with this, the two samples requiring larger Vv values of 30% (dinoflagellate and cryptophyte) display higher d_{eff} and c_i values than the two samples that can be modelled with Vv values of 20% (flagellate and diatom). To facilitate comparison between assemblages the real refractive indices of the two samples with forced Vv values of 30% were adjusted to maintain a constant homogeneous volume equivalent $1+\varepsilon$ of 1.044 – n_{chlor} values for the dinoflagellate and cryptophyte samples thus use $1+\varepsilon=1.10$ as opposed to $1+\varepsilon=1.14$ for flagellate and diatom samples.

A final comment of the refractive index determinations can be made with regard to the use of volume equivalent determinations. Figure 5e displays the n'_{chlor} values calculated both from volume equivalence with homogeneous n'_h values, and those determined directly using Aden-Kerker theory. In the majority of cases the agreement between the two methods is good, with <10% difference. The exceptions are at the Soret peak of the cryptophyte and dinoflagellate samples, where differences of ~15% and ~25% are observed. It should be remembered that the n'_h are calculated with the ADA, known to give errors of ~10% in comparison to Mie theory (Latimer, 1984; Geider and Osborne, 1987), and some discrepancies can therefore be expected between ADA and Aden-Kerker derived values. The general agreement between volume equivalent derived imaginary refractive index values and those derived from exact theory are consistent with previous discussion indicating the effects of cell heterogeneity are relatively small on absorption. It would thus seem reasonable to employ the more easily derived volume equivalent refractive index values for general cases, perhaps excepting very highly packaged cells such as the dinoflagellate sample.

Based on the Aden-Kerker derived refractive index spectra and measured algal size distributions for the four sample assemblages, the same code was used to determine a range of simulated efficiency factors and inherent optical properties for two-layered

**Phytoplankton
optical models with
two layered spheres**S. Bernard et al.

Title Page

Abstract

Introduction

Conclusions

References

Tables

Figures

◀

▶

◀

▶

Back

Close

Full Screen / Esc

Printer-friendly Version

Interactive Discussion



and volume equivalent homogeneous geometries.

5.2 Modelled optical efficiency factors

Mean optical efficiency factors are detailed in Fig. 6. Consistent with Fig. 1, it appears that geometry related differences in attenuation, total scattering and absorption are relatively small. Absorption appears to be least affected by geometry changes – heterogeneous cells produce slightly lower absorption values with a maximum 10% difference and little change in spectral shape (Fig. 6c). Attenuation differences are slightly more pronounced (Fig. 6a), with changes in spectral shape with geometry most noticeable for large cell assemblages – the two-layered geometry Q_c values appear to display greater spectral variability than their homogeneous counterparts. Maximum differences for Q_c values occur at red wavelengths and are ~15% – in all cases apart from the far red values for the dinoflagellate sample, the two-layered values are higher. Of the three non-angular efficiency factors, geometry related differences in scattering are most pronounced (Fig. 6b and e) – two-layered Q_b values are ~15% higher in most cases, with the most pronounced spectral differences observed for the dinoflagellate sample. In all cases the magnitude and spectral shape of the Q_c , Q_b , and Q_a spectra displayed in Fig. 6 are consistent with analogous published experimental data for algal cultures (Bricaud et al. 1988, Ahn et al., 1992).

The geometry related effects for attenuation, scattering and absorption are very small in comparison to those observed for backscattering. Two-layered backscattering values range from ~500 to ~2500% higher than equivalent homogeneous values, with considerable differences in spectral shape (Fig. 6d and f). Two-layered Q_{bb} values range from ~0.002 to ~0.026, in comparison to homogeneous Q_{bb} values of ~0.0002 to 0.0014. The two-layered Q_{bb} values compare well with measured Q_{bb} values for a range of algal cultures of ~0.003 to ~0.039 (Vaillancourt et al., 2004), indicating that the large increases in backscattering associated with heterogeneity are appropriate. The backscattering spectra display considerable variability with wavelength, with consistent depressions located at very slightly shorter wavelengths than the Soret and red

BGD

6, 1497–1563, 2009

Phytoplankton optical models with two layered spheres

S. Bernard et al.

Title Page

Abstract

Introduction

Conclusions

References

Tables

Figures

◀

▶

◀

▶

Back

Close

Full Screen / Esc

Printer-friendly Version

Interactive Discussion



Chl-*a* absorption peaks – such features are consistent with the effects of anomalous dispersion (Van de Hulst, 1957; Bricaud et al., 1983; Zaneveld and Kitchen, 1995), and equivalent features have been observed in measured angular scattering data (Chami et al., 2006).

Further assemblage-specific anomalous dispersion effects can be seen in the depressions at ~495 and ~550 nm in the cryptophyte sample (Fig. 6b), which correspond with the unusually distinct absorption bands at these wavelengths for this assemblage. All algal backscattering spectra display their highest values at red wavelengths, with broad secondary maxima at ~600 nm – the region where algae typically display absorption minima (e.g. Fig. 6c). These anomalous dispersion effects are not always seen in measured Q_{bb} values for algal cultures (Vaillancourt et al., 2004) – probably due to the assumptions made in the conversion factors used to calculate particulate backscattering with fixed-angle scattering sensors (Chami et al. 2006a).

The varying magnitude of the Q_{bb} spectra (Fig. 6d) are consistent with both the size effects (Fig. 4d) and the real refractive index effects (Fig. 1d) discussed previously – the two small celled samples with central values of $n_{\text{chlor}}=1.14$ (flagellate and diatom) display backscattering efficiencies 2 to 3 times higher than larger celled samples with central values of $n_{\text{chlor}}=1.10$ (dinoflagellate and cryptophyte). The decoupled effects of these variables on heterogeneous backscattering will be discussed in more detail below.

5.3 Modelled inherent optical properties

Chl-*a*-specific inherent optical properties and package effect parameter data for the four example assemblages can be seen in Fig. 7. The magnitude and spectral shape of the attenuation (Fig. 7a) and scattering (Fig. 7b) values are again consistent with previously published values for algal cultures (Bricaud et al. 1988, Ahn et al., 1992). Geometry related differences for attenuation, scattering absorption and backscattering are equivalent to those discussed above with regard to efficiency factors. Adopting a two-layered geometry results in slightly greater packaging (Fig. 7e) for all samples

Phytoplankton optical models with two layered spheres

S. Bernard et al.

Title Page

Abstract

Introduction

Conclusions

References

Tables

Figures

◀

▶

◀

▶

Back

Close

Full Screen / Esc

Printer-friendly Version

Interactive Discussion



with maximum differences of $\sim 10\%$ – the dinoflagellate sample is the most affected, as might be expected considering the relatively high d_{eff} and c_j values of this assemblage.

Chl-*a*-specific backscattering values for the two-layered geometry range from $\sim 2.0 \times 10^{-3}$ to $\sim 1 \times 10^{-4} \text{ m}^2 \text{ mg}^{-1}$ at 550 nm, as compared to homogeneous values $\sim 13 \times 10^{-4}$ to $\sim 2 \times 10^{-5} \text{ m}^2 \text{ mg}^{-1}$ at the same wavelength. These can be compared to measured ranges of $\sim 1.0 \times 10^{-3}$ to $\sim 2 \times 10^{-5} \text{ m}^2 \text{ mg}^{-1}$ at 550 nm (Ahn et al., 1992), the mean value of $9 \times 10^{-4} \text{ m}^2 \text{ mg}^{-1}$ at 510 nm (Vaillancourt et al., 2004), and a measured value for *Trichodesmium* spp. of $2.0 \times 10^{-3} \text{ m}^2 \text{ mg}^{-1}$ at 550 nm (Subramaniam et al., 1999). With the caveat that such coarse range comparisons are useful only to first order, and there are observed discrepancies with the data of Ahn et al. (1992), the comparable values of the higher two-layered values generated here and the experimental values indicates appropriate input and structure with regard to the heterogeneous model.

Modelled backscattering probability data (Fig. 7f) show equivalent geometry related differences to those discussed with regard to Fig. 6. Backscattering probability values range from ~ 0.2 to $\sim 1\%$ for the two-layered geometry, as compared to ~ 0.02 to $\sim 0.08\%$ for homogeneous particles. Such values can be compared to values determined experimentally of ~ 0.01 to $\sim 0.4\%$ (Bricaud et al., 1983; Ahn et al., 1992), those determined through combined experiment and radiative transfer modelling of ~ 0.2 to $\sim 1.5\%$ (Stramski and Piskozub, 2003), and those predicted by Mie theory of a maximum of $\sim 0.2\%$ (Bricaud et al., 1983; Morel and Bricaud, 1986; Morel, 1988). Additional comparisons can be made to particulate backscattering probabilities (although these will include the contribution of non-chlorophyllous particles) derived from fixed angle scattering meters of ~ 0.5 to $\sim 1.5\%$ for non-sediment dominated coastal waters (Twardowski et al., 2001; Sullivan et al., 2005; Whitmire et al., 2007). Accounting for the well known presence of non-chlorophyllous particulate in \tilde{b}_b values for coastal waters, the phytoplankton only \tilde{b}_b data generated here compare well, occupying the lower range of reported values as would be expected. The \tilde{b}_b data from this study also clearly show that adopting a viable heterogeneous geometry produces considerably higher

**Phytoplankton
optical models with
two layered spheres**

S. Bernard et al.

Title Page

Abstract

Introduction

Conclusions

References

Tables

Figures

◀

▶

◀

▶

Back

Close

Full Screen / Esc

Printer-friendly Version

Interactive Discussion



backscattering probabilities than homogeneous equivalents.

5.4 Size- and assemblage-dependent inherent optical properties

The assemblage-specific refractive index spectra and morphometric data can be used, in combination with the equivalent size distribution approach of Bernard et al. (2007), to calculate the optical properties of hypothetical polydispersed algal populations. This gives the ability to assess the optical effects of variability in key intracellular parameters: the imaginary and real refractive indices, and chloroplast morphology. In addition, such an approach also allows a greater understanding of the effects of changing mean assemblage size, as given by the effective diameter. Whilst such relationships are well understood as regards algal absorption, they are poorly understood with regard to algal backscattering, particularly so from the perspective of a heterogeneous geometry.

A Chl-*a*-specific size distribution for a hypothetical algal population can be calculated based on three variables: the effective diameter d_{eff} , the effective variance v_{eff} and the intracellular Chl-*a* concentration c_i . A Standard size distribution $F(d)$ for a range of particle sizes given by diameter d is expressed as (Hansen and Travis, 1974):

$$F(d) = ASF \left(\frac{d}{2} \right)^{[(1-3v_{\text{eff}})/v_{\text{eff}}]} \exp \left(\left(\frac{d}{2} \right) / \left(\frac{d_{\text{eff}}}{2} v_{\text{eff}} \right) \right) \quad (24)$$

where ASF can be treated as an arbitrary scaling parameter at this stage. The total relative particle volume \bar{V} of this distribution can then be calculated with:

$$\bar{V} = \frac{\pi}{6} \int F(d) d^3 d(d) \quad (25)$$

and the initial distribution $F(d)$ scaled to Chl-*a*-specific $F^*(d)$ with:

$$F^*(d) = \frac{F(d)}{\bar{V} c_i} \quad (26)$$

BGD

6, 1497–1563, 2009

Phytoplankton optical models with two layered spheres

S. Bernard et al.

Title Page

Abstract

Introduction

Conclusions

References

Tables

Figures

◀

▶

◀

▶

Back

Close

Full Screen / Esc

Printer-friendly Version

Interactive Discussion



The $F^*(d)$ values can then be used with the Aden-Kerker derived refractive indices discussed in Sect. 5.1, with the additional use of Eq. (21) to ensure that the chloroplast refractive index data are consistent with the c_i value employed. With this approach IOPs have been generated for hypothetical diatom and dinoflagellate populations with d_{eff} varying from 2 μm to 64 μm . Refractive index spectra from the diatom and dinoflagellate example assemblages analysed previously have been used, in combination with the measured c_i values for these assemblages of 2.3 and 4.0 kg m^{-3} , respectively. Diatom simulations employed $Vv=20\%$ and $n_{\text{chlor}}=1.14$ values, whilst dinoflagellate simulations employed $Vv=30\%$ and $n_{\text{chlor}}=1.10$ values, as deduced for the original example assemblages. Cytoplasm refractive index values are as used previously.

It must be appreciated that the use of constant refractive index and morphological data across a wide range of algal sizes is a first approximation. In reality, size and assemblage related variability will be considerably more complex, due to issues such as the non-scalability of certain intracellular membranes (Raven, 1986); photoadaptive, taxon, and trophic state induced morphological variability (Table 1); and c_i and resultant real and imaginary refractive index variability (Bricaud et al., 1988); amongst others. The use of a single chloroplast refractive index spectrum as representative of a group such as the dinoflagellates across a wide range of cell sizes is also very much a simplification, as the relative concentration and occurrence of accessory pigments will obviously vary considerably in nature. In addition the real refractive index of the chloroplast, kept at a constant central value for each assemblage across the size range, is likely to show variability (Bricaud et al., 1988; Ahn et al., 1992). Nevertheless, as a preliminary means of enhancing understanding of the optical variability of algal populations, the approach is of considerable use. Diatoms and dinoflagellates are chosen as examples due to the occurrence of these algal groups across a wide range of sizes (Table 1, Bricaud et al., 1988; Ahn et al., 1992). It should be realized that the refractive index spectra employed for these groups are representative of the measured accessory pigment suite – the dinoflagellates are thus considered representative only of those species containing peridinin as the dominant accessory pigment.

**Phytoplankton
optical models with
two layered spheres**S. Bernard et al.

[Title Page](#)[Abstract](#)[Introduction](#)[Conclusions](#)[References](#)[Tables](#)[Figures](#)[◀](#)[▶](#)[◀](#)[▶](#)[Back](#)[Close](#)[Full Screen / Esc](#)[Printer-friendly Version](#)[Interactive Discussion](#)

Phytoplankton optical models with two layered spheres

S. Bernard et al.

Title Page

Abstract

Introduction

Conclusions

References

Tables

Figures

◀

▶

◀

▶

Back

Close

Full Screen / Esc

Printer-friendly Version

Interactive Discussion



Figure 8 details the Chl-*a*-specific inherent optical properties of simulated diatom dominated populations of effective diameters from 2 to 64 μm . The changing shape of the attenuation coefficient $c_{\phi}^*(\lambda)$ with size (Fig. 8a) is of considerable interest: it has been used previously for refractive index determinations (Bricaud and Morel, 1986; Twardowski et al., 2001), and to establish estimates of particle size distribution parameters (Boss et al., 2001; Roesler and Boss, 2003). Three broad types of spectral shape in $c_{\phi}^*(\lambda)$ can be distinguished (Fig. 8a):

1. Decreasing $c_{\phi}^*(\lambda)$ with λ for small cell sizes ($d_{\text{eff}}=2$ and 4 μm);
2. Increasing $c_{\phi}^*(\lambda)$ with λ for intermediate cell sizes ($d_{\text{eff}}=8$ and 16 μm); and
3. Approximately constant $c_{\phi}^*(\lambda)$ for larger cell sizes ($d_{\text{eff}}=32$ and 64 μm) (Bricaud et al., 1986).

Such observations are not entirely consistent with studies employing numerical relationships between the attenuation and Junge slopes to describe the particle size distribution (Boss et al., 2001; Twardowski et al., 2001), which cannot display the second case of spectral shape above. However, such studies have been concerned with total particulate as opposed to the viable algal particulate (ibid.), and the inconsistency is at least in part due to this. Otherwise the changing slope and magnitude of the $c_{\phi}^*(\lambda)$ spectra with size are entirely consistent with both measurement and theory (Bricaud and Morel, 1986; Bricaud et al., 1988). Again, geometry related differences in the attenuation spectra are small (<15%), and adoption of a two-layered geometry does not appear to impact upon the spectral shape considerations discussed above. Similar considerations hold for the scattering $b_{\phi}^*(\lambda)$ spectra (Fig. 8b), which are also consistent in shape and magnitude with previous observations (ibid.). The simulated diatom Chl-*a*-specific absorption (Fig. 8c) and package effect parameter (Fig. 8e) spectra display well known characteristics with regard to changing size – higher absorption and less packaging at smaller sizes (Kirk, 1975; Morel and Bricaud, 1981; Ciotti et al., 2002). Geometry related effects are not large and vary with size – for small cells the hetero-

geneous geometry produces higher $a_{\phi}^*(\lambda)$ and $Q_a^*(\lambda)$ values (i.e. lower packaging) with a maximum difference of $\sim 10\%$. For large cells the situation is reversed – the heterogeneous geometry produces lower $a_{\phi}^*(\lambda)$ and $Q_a^*(\lambda)$ values (i.e. higher packaging) with a maximum difference of $\sim 20\%$. These are consistent with the single cell analyses of Fig. 1. The geometry related differences for small cells are also consistent with the observations of Geider and Osborne (1987), who found experimentally determined cellular packaging for a small diatom species to be lower than theoretical predictions, and ascribed the differences at least in part to cellular heterogeneity. No comparable study with regard to large cells is known to the authors. Nevertheless, the predicted absorption coefficients and package effect parameters for the simulated populations are consistent with observation (ibid.), and reveal small but significant differences arising from cellular heterogeneity.

Geometry related differences in the Chl-*a*-specific backscattering coefficient $b_{b\phi}^*(\lambda)$ (Fig. 8d) and backscattering probability $\tilde{b}_{b\phi}(\lambda)$ (not shown) are large, and similar to those discussed for Fig. 7. Heterogeneous populations produce $b_{b\phi}^*(\lambda)$ and $\tilde{b}_{b\phi}(\lambda)$ values ranging from ~ 200 to $\sim 3500\%$ higher than their homogeneous equivalents, with small celled populations exhibiting the greatest differences. Backscattering values are highest for small sizes, as is expected with Chl-*a*-specific $b_b(550) = 3.8 \times 10^{-3} \text{ m}^2 \text{ mg}^{-1}$ for the $2 \mu\text{m}$ population and $b_b(550) = 6 \times 10^{-5} \text{ m}^2 \text{ mg}^{-1}$ for the $64 \mu\text{m}$ population. Small and intermediate sized cell populations also display greater absolute spectral variability in their backscattering spectra, with spectral standard deviations ~ 5 to 10 times higher than those for larger cell populations. The normalised backscattering spectra (Fig. 8f) provide further evidence that the shape of the backscattering coefficient is strongly size-dependent, showing pronounced anomalous dispersion effects at all sizes other than the smallest diameter population. In addition, the backscattering shape at larger sizes show a pronounced broad maximum at red wavelengths – the effects of this phenomenon have been observed in the pronounced red reflectance peak in high biomass bloom waters (Carder and Steward, 1985; Gower et al., 1999; Roesler and Boss, 2003). Understanding the phenomenon is thus extremely important with regard

**Phytoplankton
optical models with
two layered spheres**S. Bernard et al.

Title Page

Abstract

Introduction

Conclusions

References

Tables

Figures

◀

▶

◀

▶

Back

Close

Full Screen / Esc

Printer-friendly Version

Interactive Discussion



to the application of bio-optical and ocean colour techniques to harmful algal bloom monitoring, where the effects of elevated algal backscattering at red wavelengths are likely to be most pronounced.

Figure 5f shows that the effect is not due to elevated real refractive index values at these wavelengths. The cause of the phenomena would appear rather to be partially due to the imaginary refractive index, or rather the lack of it – the n'_{chlor} and n'_{cyto} values at >700 nm are extremely low ($<1 \times 10^{-5}$). Figures 3 and 4 show that low imaginary refractive indices, either for the chloroplast or the entire cell, result in elevated backscattering values – this effect is considerably pronounced at very low values n'_{chlor} values, e.g. $<1 \times 10^{-5}$ (data not shown). The reason why larger cells show elevated backscattering maxima at red wavelengths in comparison to smaller cells would appear to be due to α related changes. Figure 4d (green dashed line) shows that when considering the α vs. Q_{bb} relationship for polydispersed cells with low imaginary refractive index there are three distinct regions: (1) with $\alpha < \sim 70$, Q_{bb} increases sharply with α , (2) with α between ~ 70 and ~ 400 , Q_{bb} decreases sharply with α , and (3) with $\alpha > \sim 400$, Q_{bb} decreases slowly with α . Wavelength induced changes in α across these zones, where Q_{bb} changes rapidly, will thus lead to prominent spectral features in the backscattering spectra. It must also be appreciated that small cells have narrower α ranges: a $4 \mu\text{m}$ cell would have associated α values of ~ 42 and ~ 24 at 400 and 700 nm respectively, as compared to a $32 \mu\text{m}$ cell with analogous α values of ~ 335 and ~ 192 . Large cells with low imaginary refractive index values are thus more prone to rapid increases in Q_{bb} with increasing wavelength (decreasing α) – effectively the spectral range of the Q_{bb} spectra >700 nm falls within the second region discussed above. This phenomenon, in combination with anomalous dispersion effects resulting from the high n'_{chlor} values at the red Chl-*a* peak, appear to produce the distinct backscattering maximum at red wavelengths for large celled assemblages.

There are implications to this phenomenon, with regard to both algal absorption and backscattering. Residual measured absorption at long wavelengths is often considered due to scattering, and can be corrected for using both estimates of scattering (Bricaud

**Phytoplankton
optical models with
two layered spheres**S. Bernard et al.

Title Page

Abstract

Introduction

Conclusions

References

Tables

Figures

◀

▶

◀

▶

Back

Close

Full Screen / Esc

Printer-friendly Version

Interactive Discussion



et al., 1983) and a null point correction (Roesler, 1998) – the technique adopted in this study. The absorption characteristics of algae in the near infra-red are still open to debate, not least due to the methodological difficulties of measuring low absorption values of scattering particles. Whilst some studies have concluded that algal absorption in the red is small (Babin and Stramski, 2002), others have measured residual absorption at red wavelengths that cannot be accounted for by scattering processes (Bricaud et al., 1983; Osborne and Geider, 1989). Given the sensitivity of backscattering to even small changes in the imaginary refractive index at these wavelengths, it would appear that correct measurement of algal absorption is of great importance to establishing the nature of algal backscattering at red to infra red wavelengths.

Figure 9 displays the Chl-*a*-specific inherent optical properties of simulated dinoflagellate populations of effective diameters from 2 to 64 μm . The input parameters differ to those used in Fig. 8 in that the dinoflagellate refractive index spectra are used, $c_i = 4 \text{ kg m}^{-3}$ and $V_V = 30\%$. The lower magnitudes of the $c_\phi^*(\lambda)$ (Fig. 9a) and $b_\phi^*(\lambda)$ (Fig. 9b) spectra, by comparison to the diatom simulation (Fig. 8a), are due primarily to the effects of the higher c_i value of the dinoflagellate sample. Whilst the differences between the analogous optical efficiency spectra are relatively small, the Chl-*a*-specific size distributions calculated with Eqs. (24) to (26) are $\sim 40\%$ smaller in the dinoflagellate case. In the case of absorption (Fig. 9c), the higher Q_a values resulting from the increased c_i values and larger chloroplast volume are more than offset by the smaller size distributions to produce $a_\phi^*(\lambda)$ values ranging from ~ 8 to $\sim 40\%$ smaller than those of the diatom populations. Similar considerations hold for the package effect – the dinoflagellate populations display $\sim 8\%$ greater packaging for small cells increasing to $\sim 40\%$ for the large celled assemblages. Simulated dinoflagellate backscattering (Fig. 9d) is ~ 2 to 4 times lower than that for corresponding diatom populations – this is primarily due to the higher central real refractive index value of the diatom population. The red backscattering maximum is noticeably more enhanced for the dinoflagellate populations (Fig. 9f), due to the higher relative assumed chloroplast volume of $V_V = 30\%$, leading to $Q_{bb}(700)$ values $\sim 50\%$ higher than $V_V = 20\%$ values. Given that

Phytoplankton optical models with two layered spheres

S. Bernard et al.

Title Page

Abstract

Introduction

Conclusions

References

Tables

Figures

◀

▶

◀

▶

Back

Close

Full Screen / Esc

Printer-friendly Version

Interactive Discussion



**Phytoplankton
optical models with
two layered spheres**

S. Bernard et al.

[Title Page](#)[Abstract](#)[Introduction](#)[Conclusions](#)[References](#)[Tables](#)[Figures](#)[◀](#)[▶](#)[◀](#)[▶](#)[Back](#)[Close](#)[Full Screen / Esc](#)[Printer-friendly Version](#)[Interactive Discussion](#)

the pronounced red reflectance peaks that would result from this elevated long wavelength backscattering are typically associated with very high biomass dinoflagellate blooms (Carder and Steward, 1985; Gower et al., 1999; Roesler and Boss, 2003) it is tempting to interpret these data as being typical of large celled dinoflagellates. However, this would be somewhat simplistic, particularly given that the data used here employ somewhat generalised morphological values, and that the imaginary refractive index data at red wavelengths are generated from absorption data measured in a spectral region with low signal:noise ratios and employing a null point correction. There is also considerable complexity introduced in the translation of algal spectral backscattering features into reflectance data representative of the water body as a whole. Nevertheless the enhanced red wavelength backscattering features seen here are consistent with observation and worthy of closer investigation.

6 Preliminary validation of the two-layered geometry

Absolute validation of the two-layered model would require comparison with full angular scattering measurements of cultured algal populations (e.g. Quinby-Hunt et al., 1989; Chami et al., 2006a) – such data are not available to this study. Currently commercially available backscattering instrumentation are in essence single- or multi-angle scattering meters, from which volume backscattering coefficients are calculated based upon assumptions rooted in Mie theory (Maffione and Dana, 1997; Boss et al., 2001). Validation with such instruments would require measurements of cultured algae (Vaillancourt et al., 2004) – again, such data are not available to this study. However even in such circumstances the use of these instruments would provide uncertain validation, as the Mie theory upon which their spectral backscattering derivations are based has been shown to be somewhat inappropriate to the simulation of algal angular scattering. An alternative to the use of dedicated backscattering instruments is offered by the use of reflectance data; or more accurately the often used reflectance approximation (Morel and Prieur, 1977; Zaneveld, 1995; Roesler and Perry, 1995).

This approximation, commonly used for reflectance inversion algorithms (ibid.) expresses the light leaving the sea surface in terms of the absorption and backscattering properties of the water column. Using remote sensing reflectance R_{rs} (Zaneveld, 1995)

$$R_{rs} = \frac{L_u(0^+, \lambda)}{E_d(0^+, \lambda)} = \frac{f}{Q} \frac{b_b(\lambda)}{a(\lambda) + b_b(\lambda)} \quad (27)$$

5 where $L_u(0^+, \lambda)$ is the upwelling radiance just above the sea surface, $E_d(0^+, \lambda)$ is the downwelling irradiance just above the sea surface, f/Q is an assumed constant ($=0.085$) describing the angular structure of the light field, and $a(\lambda)$ and $b_b(\lambda)$ are the total absorption and backscattering coefficients respectively. It is thus possible to relate the absorption and backscattering coefficients in the upper optical depths (Gordon and McInuney, 1975) to measurements of the upwelling radiance and downwelling irradiance. In practice, in-water reflectance measurements require that the upwelling radiance moiety is necessarily made at some nominal depth below the surface, requiring the further use of a propagation scheme to describe the attenuation of upwelled radiance as it is propagated to the surface (Albert and Mobley, 2003). Given that the diffuse attenuation coefficient for upwelling radiance can be also expressed in terms of the absorption and backscattering coefficients (ibid.), Eq. (27) can be reformulated to explicitly solve for the upwelling radiance L_u measured at depth z :

$$L_u(z, \lambda) = \frac{f}{Q} \frac{\eta^2}{\tau} \frac{b_b(\lambda)}{a(\lambda) + b_b(\lambda)} \frac{E_d(\lambda)}{\exp(-K_u(\lambda)z)} \quad (28)$$

20 where η^2/τ is an assumed constant ($=1.3612$) describing the transmittance across the air-sea interface, K_u is the diffuse attenuation coefficient for upwelling radiance and other notation is as for Eq. (27). The diffuse attenuation coefficient for upwelling radiance K_u is dependent upon the total absorption and backscattering coefficients, and solar zenith angle θ_s , using the formulation of Albert and Mobley (2003):

$$K_u = (a + b_b) \left(1 + \left(\frac{b_b}{a + b_b} \right) \right)^{3.452} \left(1 - \frac{0.2786}{\cos \theta_s} \right) \quad (29)$$

**Phytoplankton
optical models with
two layered spheres**

S. Bernard et al.

Title Page

Abstract

Introduction

Conclusions

References

Tables

Figures

◀

▶

◀

▶

Back

Close

Full Screen / Esc

Printer-friendly Version

Interactive Discussion



**Phytoplankton
optical models with
two layered spheres**

S. Bernard et al.

Title Page

Abstract

Introduction

Conclusions

References

Tables

Figures

◀

▶

◀

▶

Back

Close

Full Screen / Esc

Printer-friendly Version

Interactive Discussion



In most waters, the total absorption and backscattering coefficients will include contributions from constituents other than water itself and the algal component: these include gelbstoff, organic detritus, small particles such as bacteria, viruses and lithogenic particles, and sediment in areas of significant terrestrial input. However, algal blooms of extraordinary biomass can provide scenarios where it is not unreasonable to assume that the sea's optical properties are dominated only by algae and water, and the effects of other constituents can be regarded as negligible. This is particularly so in scenarios where there is little riverine input, such as the southern Benguela. The use of the reflectance approximation as a validation tool does suffer from some uncertainties with regard to assumptions concerning the angular structure of the light field (Zaneveld et al., 1995; Morel et al., 2002). However, it is of particular advantage to this study in that it offers a means of directly calculating the integrated backscattering coefficient, and in addition allows an assessment of the effects of adopting a more complex algal geometry on ocean colour measurements.

Under this reasoning, reflectance data from two extraordinary blooms occurring in the Lamberts Bay region of the southern Benguela are used to assess the validity of the two-layered geometry with regard to algal optics. The first of these events occurred in October 2002; a bloom of the large dinoflagellate *Alexandrium catenella*, with microscope counts taken during sampling revealing a unialgal bloom with cell concentrations of 9.8 million cells l^{-1} . The second bloom, occurring in April 2004, was of the small dinoflagellate *Prorocentrum triestinum* – microscope counts again showed a unialgal bloom with cell concentrations of 120 million cells l^{-1} . Even in a productive system suffering the frequent occurrence of high biomass dinoflagellate blooms (Pitcher et al., 1998), these events were conspicuous both by their magnitude and monospecific nature.

6.1 Methods for radiance comparisons

Principal measurements consist of in-water hyperspectral radiometric measurements, and algal microscopic counts and size calculations used to derive algal size distribu-

tions. Radiometric measurements were made with two in-water hyperspectral instrument systems. Measurements of the *A. catenella* bloom utilised a Satlantic Hyperspectral Tethered Surface Radiometer Buoy (H-TSRB) – a tethered surface buoy measuring upwelling radiance at a nominal depth of 0.66 m, and above surface downwelling irradiance. The *P. triestinum* bloom was measured using a TRIOS ACC sensor, measuring downwelling above surface irradiance, and a TRIOS ARC radiance sensor measuring upwelling radiance at a nominal depth of 0.4 m. The TRIOS sensors were mounted on a prototype coastal bio-optical monitoring buoy, using a modified Ocean-i power and data control system (Saturn Solutions, UK). The two systems can be considered approximately analogous with regard to measurement geometry and radiometric sensitivity, and both have a spectral resolution of ~ 3 nm. Radiometric measurements were made for a duration of two to five minutes, with sampling rates (dictated by radiance integration times) of ~ 0.5 Hz. Median values from the whole sampling period were used to derive single spectra for both sensors, resampled to a wavelength resolution of 5 nm. Microscope counts were made on samples preserved with buffered formalin and counted using the Utermohl (1958) technique. Mean equivalent volume spherical cell diameters were calculated based on ~ 40 microscope measurements of cell dimensions, utilizing a spheroidal geometry to calculate cell volume.

Modelled upwelling radiance spectra are calculated using several steps: Standard size distributions (Bernard et al., 2007), were generated using the microscope cell concentration and d_{eff} data, using an effective variance of $v_{\text{eff}}=0.006$ – the narrowest possible numerically stable distribution using the Hansen and Travis (1974) formulation.

The integrated total number of particles for each distribution were forced to match reported cell concentration values of 9.8×10^9 cells m^{-3} for the *A. catenella* bloom and 1.2×10^{11} cells m^{-3} for the *P. triestinum* bloom. Equation (12) was then used to calculate algal absorption and backscattering properties using the microscope-derived size distribution and optical efficiency factors modeled from the dinoflagellate refractive index data (Fig. 5e and f). Optical data for two-layered cells with chloroplast volumes of $V_V=20\%$ and $V_V=30\%$ were generated, in addition to data for a volume equivalent

Phytoplankton optical models with two layered spheres

S. Bernard et al.

Title Page

Abstract

Introduction

Conclusions

References

Tables

Figures

◀

▶

◀

▶

Back

Close

Full Screen / Esc

Printer-friendly Version

Interactive Discussion



homogeneous geometry.

Equation (28) was then used to calculate simulated upwelling radiance spectra, using measured downwelling irradiance spectra, the modelled algal absorption and backscattering coefficients, and the absorption and backscattering of water. For the absorption of pure water the data of Pope and Fry (1997) were used for 400 nm to 725 nm, with scaled data from Buiteveld et al. (1994) used for 730 nm to 750 nm. The equations of Morel (1974) were used to generate pure seawater backscattering coefficients.

6.2 Results of radiance comparisons

Microscope-derived size distributions can be seen in Figs. 10e and 11e, based on calculated effective diameter values of $d_{\text{eff}}=30\ \mu\text{m}$ for *A. catenella* and $d_{\text{eff}}=13\ \mu\text{m}$ for *P. triestinum*. The Standard distribution for the *A. catenella* sample (using the smallest possible numerically stable v_{eff} value) appears rather wide for a unialgal event, and simulations were checked using normal and log-normal distributions allowing considerably narrower distributions – reflectance perturbations with narrower size distributions were relatively minor (<10%).

The measured upwelling radiance spectra (Figs. 10a and 11a) can be considered typical of very high biomass waters, and are characterized by low light levels in the blue and a red peak located at >700 nm. This peak must be distinguished from the sun induced natural fluorescence peak (Babin et al., 1996), typically located at ~683 nm. As concerns the *A. catenella* simulations in Fig. 10, the simulated radiance data show a reasonable match to measured data, with considerable geometry-related variability. Given the very low radiance values below ~550 nm and between ~660 nm and ~680 nm, comparisons will be restricted to values at the two main radiance peaks, located at ~580 nm and ~710 nm. The two-layered $V_V=20\%$ data would appear the best matched geometry, with a relative underestimate of ~10% at 580 nm and a relative overestimate of ~80% at 710 nm. In comparison the two-layered $V_V=30\%$ data appear to backscatter too strongly in the red (Fig. 10c), overestimating reflectance at 710 nm by >100%. This is consistent with previous discussions of morphologically in-

BGD

6, 1497–1563, 2009

Phytoplankton optical models with two layered spheres

S. Bernard et al.

Title Page

Abstract

Introduction

Conclusions

References

Tables

Figures

◀

▶

◀

▶

Back

Close

Full Screen / Esc

Printer-friendly Version

Interactive Discussion



duced variability in the red backscattering phenomena, and indicates the importance of the assumed morphology in such an approach. The homogeneous geometry underestimates radiance by $\sim 80\%$ at both radiance peaks. Comparison of the absorption (Fig. 10b) and backscattering (Fig. 10c) data show that geometry-related absorption variability is small ($<15\%$) in comparison to backscattering variability, where the homogeneous geometry produces b_b values ~ 20 to 60% lower than those of the heterogeneous b_b values. In comparison to the *A. catenella* bloom, the *P. triestinum* event showed much higher cell concentrations of a smaller organism ($d_{\text{eff}}=13\ \mu\text{m}$), leading to a relatively high red wavelength radiance peak. The geometry-related differences are even more marked than for the previous assemblage, with the homogeneous cells underestimating measured radiance by up to 100% . The comparison between the two heterogeneous geometries is not as marked as for the previous assemblage (~ 5 to 30% differences at 580 and $710\ \text{nm}$), although it would appear once again that the $V/V=20\%$ geometry is more appropriate, as it provides a slightly closer match to the measured radiance in the 580 to $650\ \text{nm}$ range. Again geometry-related differences in absorption (Fig. 11b) are small ($<10\%$), whilst backscattering differences are considerable, with the homogeneous geometry yielding backscattering values up to 95% lower than those of the heterogeneous geometry. The close match of the measured and simulated radiance using the heterogeneous geometries, and the poor match using the homogeneous geometry, would suggest that the two-layered geometry as it is configured here is appropriate for algal bio-optical applications.

Whilst the reflectance approach does allow the ability to confirm that the magnitude of backscattering is within appropriate ranges, the very low radiance at blue wavelengths does not allow an assessment of the simulated backscattering spectral shape throughout the visible spectrum. Nevertheless, the reasonable simulated radiance comparisons from ~ 550 to $750\ \text{nm}$, with backscattering spectra that display considerable anomalous dispersion effects (Fig. 11c) at these wavelengths, indicates that the highly structured backscattering spectra that are predicted by theory are not unreasonable. The data used in the simulation are derived from a combination of theoretical

BGD

6, 1497–1563, 2009

Phytoplankton optical models with two layered spheres

S. Bernard et al.

Title Page

Abstract

Introduction

Conclusions

References

Tables

Figures

◀

▶

◀

▶

Back

Close

Full Screen / Esc

Printer-friendly Version

Interactive Discussion



considerations, literature derived values, and absorption and size measurements from a dinoflagellate assemblage measured several years before the bloom events shown above. The close comparison between measured and simulated radiance data, based solely on the derived optical efficiency factors and microscope-derived size parameters, confirms the validity of the approach and the general application of heterogeneous geometry algal optics to in-water bio-optical application.

7 Conclusions

The study has outlined a general structure for the simulation of algal optical properties using two-layered geometry models. An initial analysis of the effects of manipulating causal variables on algal IOPs has been conducted. The adopted structure uses an inner layer representing the cytoplasm, which typically occupies most of the cell volume, and an outer layer representing the chloroplast (or chloroplasts). The model geometry has been shown to be appropriate using several arguments: it is appropriately packaged from a physiological perspective, it is able to simulate observed absorption efficiency factors, it has intracellular real refractive index gradients more closely approximating those geometries explicitly considering an optically “hard” peripheral cellular membrane, and there is a considerable body of morphological observations supporting the assumption of peripheral chloroplast location. Appropriate relative volume and refractive index ranges have been established for algal chloroplasts and cytoplasm; from a volume equivalent perspective these values are consistent with previous observation, both from a cellular composition and an optical perspective. Based on these data and field measurements of algal absorption and size distributions, chloroplast refractive index spectra have been derived for several algal assemblages typical of the Benguela system. These data have been used to assess the changing nature of algal optical efficiency factors and inherent optical properties with regard to cellular heterogeneity, and changes in assemblage size and composition.

It appears that the adoption of two-layered geometry has a relatively minor impact

BGD

6, 1497–1563, 2009

Phytoplankton optical models with two layered spheres

S. Bernard et al.

Title Page

Abstract

Introduction

Conclusions

References

Tables

Figures

◀

▶

◀

▶

Back

Close

Full Screen / Esc

Printer-friendly Version

Interactive Discussion



upon optical properties that are not dependent upon angular scattering processes – attenuation, total scattering and absorption properties, including the package effect parameter. These findings are supported by previous modeling studies (Aas, 1984; Zaneveld and Kitchen, 1995), and are generally consistent with the widespread and successful use of the anomalous diffraction approximation and Mie modeling to describe non-angular optical properties. However, angular scattering properties, of which the integrated backscattering is focused on here, are considerably affected by the adoption of a heterogeneous geometry. Algal backscattering coefficients associated with a heterogeneous geometry are between 5 and 25 times higher than their homogeneous volume equivalent counterparts; considerable differences in the spectral shape of the backscattering spectra are also induced by geometry change. The nature of these geometry-related differences vary considerably with size and intracellular refractive index.

Assessment of the size and assemblage-specific inherent optical properties show that non-angular coefficients behave consistently with previous observation and theory – examples include the changing slope of the attenuation coefficient with size, and package effect related variability in the absorption coefficient. In an analogous manner, variability in the algal backscattering coefficient can be characterized: spectral variability can be large and is size dependent, populations dominated by small cells backscatter considerably more than those dominated by large cells, and the real refractive index of the chloroplast (or equivalent peripheral layer) is the dominant influence on backscattering. It must be realised that this study makes somewhat simplistic assumptions with regard to algal morphology and intracellular refractive index values, and must be regarded as a preliminary attempt to create a general heterogeneous geometry for the simulation of spectral algal optical properties. Further data are needed, particularly with regard to the intracellular refractive index and intracellular morphology of algal groups from a systematic perspective. Nevertheless, the reflectance based validation indicates the validity of the adopted backscattering geometry and refractive index structure, and indicates that it is possible to establish a quantitative formulation

BGD

6, 1497–1563, 2009

Phytoplankton optical models with two layered spheres

S. Bernard et al.

Title Page

Abstract

Introduction

Conclusions

References

Tables

Figures

◀

▶

◀

▶

Back

Close

Full Screen / Esc

Printer-friendly Version

Interactive Discussion



between single particle optics and ocean colour. Such an approach offers the ability to express the algal contribution to in situ or remotely measured ocean colour data purely in terms of a population of particles, or more importantly for phytoplankton dynamics related applications, population size and accessory pigment related refractive index variability. Further application of the approach will be explored in harmful algal bloom oriented inverse-reflectance models; the combined use of particle size distributions with the heterogeneous geometry can establish size and assemblage-specific, coupled and easily manipulated algal absorption and backscattering coefficients.

References

- 10 Aas, E.: Influence of shape and structure on light scattering by marine particles, Report of Department of Geophysics, University of Oslo, 53, 1984.
- Aas, E.: Refractive index of phytoplankton derived from its metabolite composition, *J. Plankton Res.*, 18, 2223–2249, 1996.
- Aden, A. L., and Kerker, M.: Scattering of electromagnetic waves from two concentric spheres, *J. Appl. Phys.*, 22, 1242–1246, 1951.
- 15 Ahn, Y-H., Bricaud, A., and Morel, A.: Light backscattering efficiency and related properties of some phytoplankters, *Deep-Sea Res.*, 39A, 1835–1855, 1992.
- Albert, A. and Mobley, C. D.: An analytical model for subsurface irradiance and remote sensing reflectance in deep and shallow case-2 waters, *Opt. Express*, 11, 2873–2890, 2003.
- 20 Andersson, P. O., Gillbro, T., Ferguson, L., and Cogdell, R. J.: Absorption spectral shift of carotenoids related to medium polarizability, *Photochem. Photobiol.*, 54, 353–360, 1991.
- Babin, M., Morel, A. and Gentili, B.: Remote sensing of surface Sun-induced chlorophyll fluorescence: consequences of natural variations in the optical characteristics of phytoplankton and the quantum yield of chlorophyll a fluorescence, *Int. J. Remote Sens.*, 17, 2417–2448, 1996.
- 25 Babin, M. and Stramski, D.: Light absorption by aquatic particles in the near-infrared spectral region, *Limnol. Oceanogr.*, 47, 911–915, 2002.
- Barlow, R. G., Cummings, D. G., and Gibb, S. W.: Improved resolution of mono- and divinyl

Phytoplankton optical models with two layered spheres

S. Bernard et al.

Title Page

Abstract

Introduction

Conclusions

References

Tables

Figures

◀

▶

◀

▶

Back

Close

Full Screen / Esc

Printer-friendly Version

Interactive Discussion



chlorophylls a and b and zeaxanthin and lutein in phytoplankton extracts using reverse phase C-8 HPLC, Mar. Ecol.-Prog. Ser., 161, 303–307, 1997.

Bernard, S., Probyn, T. A., and Barlow, R. G.: Measured and modelled optical properties of particulate matter in the southern Benguela, S. Afr. J. Sci., 97, 410–420, 2001.

5 Bernard, S., Shillington, F. A., and Probyn, T. A.: The use of equivalent size distributions of natural phytoplankton assemblages for optical modeling, Opt. Express, 15, 1995–2007, 2007.

Berner, T., Dubinsky, Z., Wyman, K., and Falkowski, P. G.: Photoadaptation and the package effect in *Dunaliella tertiolecta* (Chlorophyceae), J. Phycol., 25, 70–7, 1989.

Bohren, C. F., and Huffman, D. R.: Absorption and scattering of light by small particles, John Wiley and Sons, New York, 1983.

10 Boss, E., Pegau, W. S., Gardner, W. D., Zaneveld, J. R. V., Barnard, A.H., Twardowski, M. S., Chang, G. C., and Dickey, T. D.: Spectral particulate attenuation in the bottom boundary layer of a continental shelf, J. Geophys. Res., 106(C5), 9509–9516, 2001.

Boss, E., Twardowski, M. S., and Herring, S.: Shape of the particulate beam attenuation spectrum and its inversion to obtain the shape of the particulate size distribution, Appl. Optics, 40, 4885–4893, 2001a.

15 Bricaud, A., Morel, A., and Prieur, L.: Optical efficiency factors of some phytoplankters, Limnol. Oceanogr., 28, 816–832, 1983.

Bricaud, A. and Morel, A.: Light attenuation and scattering by phytoplanktonic cells: a theoretical modeling, Appl. Optics, 25, 571–580, 1986.

20 Bricaud, A., Bedhomme, A. L., and Morel, A.: Optical properties of diverse phytoplanktonic species: experimental results and theoretical interpretation, J. Plankton Res., 10, 851–873, 1988.

Bricaud, A., Zaneveld, J. R. V., and Kitchen, J. C.: Backscattering efficiency of coccolithophorids: use of a three-layered sphere model. pp 27–33, In: Ocean Optics XI Proc SPIE, edited by: Gilbert, G. D., 1992.

25 Bricaud, A., Babin, M., Morel, A., and Claustre, H.: Variability in the chlorophyll-specific absorption coefficients of natural phytoplankton: Analysis and parameterization, J. Geophys. Res., 100, 13321–13332, 1995.

30 Bryant F. D., Seiber, A., and Latimer, B. A.: Absolute optical cross sections of cells and chloroplasts, Arch. Biochem. Biophys., 135, 97–108, 1969.

Buiteveld, H., Hakvoort, J. M. H., and Donze, M.: The optical properties of pure water. Pp 174–183, In: SPIE Proceedings on Ocean Optics XII, edited by: Jaffe, J. S., 1994.

BGD

6, 1497–1563, 2009

Phytoplankton optical models with two layered spheres

S. Bernard et al.

Title Page

Abstract

Introduction

Conclusions

References

Tables

Figures

◀

▶

◀

▶

Back

Close

Full Screen / Esc

Printer-friendly Version

Interactive Discussion



- Caffarri, S., Croce, R., Breton, J., and Bassi, R.: The major antenna complex of photosystem II has a xanthophyll binding site not involved in light harvesting, *J. Biol. Chem.*, 276, 35924–35933, 2001.
- 5 Carder, K. L. and Steward, R. G.: A remote-sensing reflectance model of a red-tide dinoflagellate off west Florida, *Limnol. Oceanogr.*, 30, 286–298, 1985.
- Chami, M., Shybanov, E. B., Khomenko, G., Lee, M., Martynov, O. V., and Korotaev, G.: Spectral variation of the volume scattering function measured over the full range of scattering angles in a coastal environment, *Appl. Optics*, 45, 3605–3619, 2006.
- 10 Chami, M., Marken, E., Stamnes, J. J., Khomenko, G., and Korotaev, G.: Variability of the relationship between the particulate backscattering coefficient and the volume scattering function measured at fixed angles, *J. Geophys. Res.*, 111, C05013, doi:10.1029/2005JC003230, 2006a.
- Charney, E. and Brackett F. S.: The spectral dependence of scattering from a spherical alga and its implications for the state of organization of the light-accepting pigments, *Arch. Biochem. Biophys.*, 92, 1–12, 1961.
- 15 Chylek, P. and Videen, G.: Scattering by a composite sphere and effective medium approximations, *Opt. Commun.*, 146: 15–20, 1998.
- Cinque, G., Croce, R., Holzwarth, A. R., and Bassi, R.: Förster energy transfer in the chlorophyll a/b complex CP29, *Biophys. J.*, 79, 1706–1717, 2000.
- 20 Ciotti, A. M., Lewis, M. R., and Cullen, J. J.: Assessment of the relationships between dominant cell size in natural phytoplankton communities and the spectral shape of the absorption coefficient, *Limnol. Oceanogr.*, 47, 404–417, 2002.
- Dodge, J. D. and Crawford, R. M.: Observations on the fine structure of the eyespot and associated organelles in the dinoflagellate *Glenodinium foliaceum*, *J. Cell Sci.*, 5, 479–493, 1969.
- 25 Dunn, A. K.: Modelling of light scattering from inhomogeneous biological cells, 19–29, in: *Optics of Biological Particles*, edited by: Hoekstra, A. G. and Maltsev, V. P., and Videen G., 2007.
- Finkel, Z. V. and Irwin, A. J.: Modelling size-dependent photosynthesis: light absorption and the allometric rule, *J. Theor. Biol.*, 204, 361–369, 2000.
- 30 Fisher, T., Berner T., Iluz D., and Dubinsky, Z.: The kinetics of the photoacclimation response of *Nannochloropsis* sp. (Eustigmatophyceae): a study of changes in ultrastructure and psu density, *J. Phycol.*, 34, 818–824, 1998.

**Phytoplankton
optical models with
two layered spheres**S. Bernard et al.

[Title Page](#)[Abstract](#)[Introduction](#)[Conclusions](#)[References](#)[Tables](#)[Figures](#)[◀](#)[▶](#)[◀](#)[▶](#)[Back](#)[Close](#)[Full Screen / Esc](#)[Printer-friendly Version](#)[Interactive Discussion](#)

- Garver, S. A. and Siegel, D. A.: Inherent optical property inversion of ocean color spectra and its biogeochemical interpretation. 1: Time series from the Sargasso Sea, *J. Geophys. Res.*, 102, 18607–18625, 1997.
- Gastrich, M. D., Anderson, O. R., Benmayor, S. S., and Coper, E. M.: Ultrastructural analysis of viral infection in the brown-tide alga, *Aureococcus anophagefferens* (Pelagophyceae), *Phycologia*, 37, 300–306, 1998.
- Geider, R. J. and Osborne, B. A.: Light absorption by a marine diatom: Experimental observations and theoretical calculations of the package effect in a small *Thalassiosira* species, *Mar. Biol.*, 96, 299–308, 1987.
- Gordon, H. R. and McLuney, W. R.: Estimation of the depth of sunlight penetration in the sea for remote sensing, *Appl. Optics*, 14, 413–416, 1975.
- Gower, J. F. R., Doerffer, R., and Borstad, G. A.: Interpretation of the 685 nm peak in water-leaving radiance spectra in terms of fluorescence, absorption and scattering, and its observation by MERIS, *Int. J. Remote Sens.*, 9, 1771–1786, 1999.
- Green, J. C.: The fine structure of *Pavlova pinguis* Green and a preliminary survey of the order Pavloales (Prymnesiophyceae), *Brit. Phycol. J.*, 15, 151–191, 1980.
- Green, R. E., Sosik, H. M., Olson, R. J., and DuRand, M. D.: Flow cytometric determination of size and complex refractive index for marine particles: comparison with independent and bulk estimates, *Appl. Opt.*, 42, 526–541, 2003.
- Gruszecki, W. I., Grudzinski, W., Banaszek-Glos, A., Matula, M., Kernen, P., Krupa, Z., and Siewiewsiuk, J.: Xanthophyll pigments in light-harvesting complex II in monomolecular layers: localisation, energy transfer and orientation, *Biochim. Biophys. Acta*, 1412, 173–183, 1999.
- Gustafson, D. E., Stoecker, D. K., Johnson, M. D., Van Heukelem, W. F., and Sneider, K.: Cryptophyte algae are robbed of their organelles by the marine ciliate *Mesodinium rubrum*, *Nature*, 405, 1049–1052, 2000.
- Hansen, J. E., and Travis, L. D.: Light scattering in planetary atmospheres, *Space Sci. Rev.*, 16, 527–610, 1974.
- Highfill, J. F. and Pfiester, L. A.: The sexual and asexual life cycle of *Glenodiniopsis steinii* (Dinophyceae), *Am. J. Bot.*, 1992, 899–903, 1992.
- Hitchcock, G. L.: A comparative study of the size-dependent organic composition of marine diatoms and dinoflagellates, *J. Plankton Res.*, 4, 363–377, 1982.
- Hoops, H. J. and Floyd, G. L.: Ultrastructure of the centric diatom, *Cyclotella meneghiniana*:

**Phytoplankton
optical models with
two layered spheres**S. Bernard et al.

Title Page

Abstract

Introduction

Conclusions

References

Tables

Figures

◀

▶

◀

▶

Back

Close

Full Screen / Esc

Printer-friendly Version

Interactive Discussion



- Vegetative cell and auxospore development, *Phycologia*, 18, 424–435, 1979.
- Hutchings, L., Pitcher, G. C., Probyn, T. A., and Bailey, G. W.: The Chemical and Biological Consequences of Coastal Upwelling. pp. 65–82, In: Dahlem Workshop on Upwelling in the Ocean: Modern Processes and Ancient Records, edited by: Summerhayes, C. P., Emeis, K. C., Angel, M. V., Smith, R. L., and Zeitzschel, B., 1994.
- Iturriaga, R. and Siegel, D. A.: Microphotometric characterization of phytoplankton and detrital absorption properties in the Sargasso Sea, *Limnol. Oceanogr.*, 34, 1706–1726, 1989.
- Janssen, M., Bathke, L., Marquardt, J., Krumbein, W. E., and Rhiel, E.: Changes in the photosynthetic apparatus of diatoms in response to low and high light intensities, *Int. Microbiol.*, 4, 27–33, 2001.
- Jeffrey, S. W. and Vesk, M.: Effect of blue-green light on photosynthetic pigments and chloroplast structure in the marine diatom *Stephanopyxis turbis*, *J. Phycol.*, 13, 271–279, 1977.
- Jenks, A. and Gibbs, S. P.: Immunolocalization and distribution of Form II Rubisco in the pyrenoid and chloroplast stroma of *Amphidinium carterae* and Form I Rubisco in the symbiont-derived plastids of *Peridinium foliaceum* (Dinophyceae), *J. Phycol.*, 36, 127–138, 2000.
- Jennings, R. C. and Zucchelli, G.: The influence of membrane stacking on light absorption by chloroplasts, *Photobioch. Photobiop.*, 9, 215–221, 1985.
- Johnsen, G., Samset, O., Granskog, L., and Sakshaug, E.: In vivo absorption characteristics in 10 classes of bloom-forming phytoplankton: taxonomic characteristics and responses to photoadaptation by means of discriminant and HPLC analysis, *Mar. Ecol.-Prog. Ser.*, 105, 149–157, 1994.
- Kirk, J. T. O.: A theoretical analysis of the contribution of algal cells to the attenuation of light within natural waters. II. Spherical cells, *New Phytol.*, 75, 21–36, 1975.
- Kishino, M., Takahashi, M., Okami, N., and Ichimura, S.: Estimation of the spectral absorption coefficients of phytoplankton in the sea, *Bull. Mar. Sci.*, 37, 634–642, 1985.
- Kitchen, J. C., Zaneveld, J. R. V., and Pak, H.: Effect of particle size distribution and chlorophyll content on beam attenuation spectra, *Appl. Opt.*, 21, 3913–3918, 1982.
- Kitchen, J. C., and Zaneveld, J. R. V.: A three-layered sphere model of the optical properties of phytoplankton, *Limnol. Oceanogr.*, 37, 1680–90, 1992.
- Kleima, F. J., Hofmann, E., Gobets, B., van Stokkum, I. H. M., van Grondelle, R., Diederichs, K., and van Amerongen, H.: Forster excitation energy transfer in peridinin-chlorophyll-*a*-protein, *Biophys. J.*, 78, 344–353, 2000.

BGD

6, 1497–1563, 2009

Phytoplankton optical models with two layered spheres

S. Bernard et al.

Title Page

Abstract

Introduction

Conclusions

References

Tables

Figures

◀

▶

◀

▶

Back

Close

Full Screen / Esc

Printer-friendly Version

Interactive Discussion



- Latimer, P.: Light scattering by a homogeneous sphere with radial projections, *Appl. Optics* 23, 442–447, 1984.
- Maffione, R. A. and Dana, D. R.: Instruments and methods for measuring the backward-scattering coefficient of ocean waters, *Appl. Opt.*, 36, 6057–67, 1997.
- 5 Malone, T. C.: Algal size, 433–463, in: *The Physiological Ecology of Phytoplankton*, edited by: Morris, I., 1980.
- Messer, G. and Ben-Shaul, Y.: Changes in chloroplast structure during culture growth of *Peridinium cinctum* fa. *westii* (Dinophyceae), *Phycologia*, 11, 291–299, 1972.
- Meyer, R. A.: Light scattering from biological cells: dependence of backscatter radiation on membrane thickness and refractive index, *Appl. Opt.*, 18, 585–588, 1979.
- 10 Mie, G.: Contribution to the optical properties of turbid media, in particular of colloidal suspensions of metals, *Ann. Phys.*, 25, 377–452, 1908.
- Moal, J., Martin-Jezequel, V., Harris, R. P., Samain, J. F., and Poulet, S. A.: Interspecific and intraspecific variability of chemical composition of marine phytoplankton, *Oceanol. Acta*, 10, 339–346, 1987.
- 15 Montagnes, D. J. S., Berges, J. A., Harrison, P. J., and Taylor, F.J.R.: Estimating carbon, nitrogen, protein, and chlorophyll a from cell volume in marine phytoplankton, *Limnol. Oceanogr.*, 39, 1044–1060, 1994.
- Morel, A.: Optical properties of pure water and pure seawater, pp. 1–24, in: *Optical aspects of oceanography*, edited by: Jerlov, N. G. and Steeman Nielsen, E., 1974.
- 20 Morel, A. and Prieur, L.: Analysis of variations in ocean color, *Limnol. Oceanogr.*, 22, 709–722, 1977.
- Morel, A. and Bricaud, A.: Theoretical results concerning light absorption in a discrete medium, and application to specific absorption of phytoplankton, *Deep-Sea Res.*, 28, 1375–1393, 1981.
- 25 Morel, A. and Bricaud, A.: Inherent properties of algal cells including picoplankton: theoretical and experimental results, *Can. Bull. Fish. Aquat. Sci.*, 214, 521–559, 1986.
- Morel, A., Antoine, D., and Gentili, B.: Bidirectional reflectance of oceanic waters: Accounting for Raman emission and varying particle phase function, *Appl. Optics*, 41, 6289–6306, 2002.
- 30 Morel, A. and Gentili, B.: Radiation transport within oceanic (case 1) water, *J. Geophys. Res.*, 109, C06008, doi:10.1029/2003JC002259, 2004.
- Muller-Parker, G., Lee, K. W., and Cook, C. B.: Changes in the ultrastructure of symbiotic zooxanthellae (*Symbiodinium* sp., Dinophyceae) in fed and starved sea anemones (*Aiptasia*

BGD

6, 1497–1563, 2009

**Phytoplankton
optical models with
two layered spheres**

S. Bernard et al.

Title Page

Abstract

Introduction

Conclusions

References

Tables

Figures

◀

▶

◀

▶

Back

Close

Full Screen / Esc

Printer-friendly Version

Interactive Discussion



**Phytoplankton
optical models with
two layered spheres**

S. Bernard et al.

[Title Page](#)[Abstract](#)[Introduction](#)[Conclusions](#)[References](#)[Tables](#)[Figures](#)[◀](#)[▶](#)[◀](#)[▶](#)[Back](#)[Close](#)[Full Screen / Esc](#)[Printer-friendly Version](#)[Interactive Discussion](#)

pallida) maintained under high and low light, J. Phycol., 32, 987–994, 1996.

Naqvi K. R., Merzlyak, M. N., and Melø, T. B.: Absorption and scattering of light by suspensions of cells and subcellular particles: an analysis in terms of Kramers-Kronig relations, Photochem. Photobio. S., 3(1), 132–137, 2004.

5 Nelder, J. A., and Mead, R.: A simplex method for function minimization, Comput. J., 7, 308–313, 1965.

Osborne, B. A. and Geider, R. J.: Problems in the assessment of the package effect in five small phytoplankters, Mar. Biol., 100, 151–159, 1989.

10 Paillotin, G., Leibl, W., Gapinski, J., Breton, J., and Dobek, A.: Light gradients in spherical photosynthetic vesicles, Biophys. J., 75, 124–133, 1998.

Pitcher, G. C., Boyd, A. J., Horstman, D. A., and Mitchell-Innes, B.A.: Subsurface dinoflagellate populations, frontal blooms and the formation of red tide in the southern Benguela upwelling system, Mar. Ecol.-Prog. Ser., 172, 253–264, 1998.

15 Pitcher G. C., Bernard, S., and Pienaar, R. N.: Brown tides on the west coast, IOC Harmful Algae News, 18, 8–10, 1999.

Pitcher, G. C. and Calder, D.: Harmful algal blooms of the southern Benguela current: A review and appraisal of monitoring from 1989 to 1997, S. Afr. J. Mar. Sci., 22, 255–271, 2000.

Pope, R. M. and Fry, E. S.: Absorption spectrum (380–700 nm) of pure water. II. Integrating cavity measurements. Appl. Optics, 36, 8710–8723, 1997.

20 Preisendorfer, R. W.: Hydrologic optics, vol. 5. Properties, US Environmental Research Laboratories, 1976.

Quinby-Hunt, M. S., Hunt, A. J., Lofftus, K., and Shapiro, D.: Polarized-light scattering studies of marine *Chlorella*, Limnol. Oceanogr., 34, 1587–1600, 1989.

25 Quirantes, A. and Bernard, S.: Light scattering by marine algae: two-layer spherical and non-spherical models, Journal of Quantitative Spectroscopy and Radiative Transfer, 89, 311–321, 2004.

Raven, J. A.: A cost-benefit analysis of photon absorption by photosynthetic unicells, New Phytol., 98, 593–625, 1984.

30 Raven, J. A.: Physiological consequences of extremely small size for autotrophic organisms in the sea, Can. Bull. Fish. Aquat. Sci., 214, 1–70, 1986.

Renge, I., van Grondelle, R., and Dekker, J. P.: Matrix and temperature effects on absorption spectra of β -carotene and pheophytin a in solution and in green plant photosystem II, J. Photochem. Photobio. A, 96, 109–121, 1996.

**Phytoplankton
optical models with
two layered spheres**

S. Bernard et al.

[Title Page](#)[Abstract](#)[Introduction](#)[Conclusions](#)[References](#)[Tables](#)[Figures](#)[◀](#)[▶](#)[◀](#)[▶](#)[Back](#)[Close](#)[Full Screen / Esc](#)[Printer-friendly Version](#)[Interactive Discussion](#)

Roesler, C. S. and Perry, M. J.: In situ phytoplankton absorption, fluorescence emission, and particulate backscattering spectra determined from reflectance, *J. Geophys. Res.*, C100, 13279–13294, 1995.

Roesler, C. S.: Theoretical and experimental approaches to improve the accuracy of particulate absorption coefficients derived from the quantitative filter technique, *Limnol. Oceanogr.*, 43, 1649–1660, 1998.

Roesler, C. S. and Boss, E.: Spectral beam attenuation coefficient retrieved from ocean colour inversion, *Geophys. Res. Lett.*, 30, 1468–1471, 2003.

Rosen, B. H. and Lowe, R. L.: Physiological and ultrastructural responses of *Cyclotella meneghiniana* (Bacillariophyta) to light intensity and nutrient limitation, *J. Phycol.*, 20, 173–183, 1984.

Rosen, B. H., Berliner, M. D., and Petro, M. J.: Analysis of starch content in *Chlorella pyrenoidosa* (Chlorophyta) by morphological and quantitative techniques, *Am. J. Bot.*, 73, 1372–1375, 1986.

Sicko-Goad, L. and Stoermer, E. F.: A morphometric study of lead and copper effects on *Diatoma tenue* var. *elongatum* (Bacillariophyta), *J. Phycol.*, 15, 316–321, 1979.

Spector, D. L. and Triemer, R. E.: Ultrastructure of the dinoflagellate *Peridinium cinctum* f. *ovoplanum*. I. Vegetative cell structure, *Am. J. Bot.*, 66, 845–850, 1979.

Stephens, F. C.: Variability of spectral absorption efficiency within living cells of *Pyrocystis lunula* (Dinophyta), *Mar. Biol.*, 122, 325–331, 1995.

Stramski, D. and Piskozub, J.: Estimation of scattering error in spectrophotometric measurements of light absorption by aquatic particles from 3-D radiative transfer equations, *Appl. Optics*, 42, 3634–46, 2003.

Stramski, D.: Refractive index of planktonic cells as a measure of intracellular carbon and chlorophyll a content, *Deep-Sea Res.*, 46, 335–351, 1999.

Stramski, D., Morel, A., and Bricaud, A.: Modelling the light attenuation and scattering by spherical phytoplankton cells: a retrieval of the bulk refractive index, *Appl. Optics*, 27, 2954–3956, 1988.

Stramski, D., Bricaud, A., and Morel, A.: Modeling the inherent optical properties of the ocean based on the detailed composition of planktonic community, *Appl. Optics*, 40, 2929–2945, 2001.

Subramaniam, A., Carpenter, E. J., and Falkowski, P. G.: Bio-optical properties of the marine diazotrophic cyanobacteria *Trichodesmium* sp. II. A reflectance model for remote sensing,

- Limnol. Oceanogr., 44, 618–627, 1999.
- Sullivan, J. M., Twardowski, M. S., Donaghay, P. L., and Freeman, S.A.: Use of optical scattering to discriminate particle types in coastal waters, *Appl. Optics*, 44, 1667–1680, 2005.
- Svensen, Ø., Frette, Ø., and Erga, S. R.: Scattering properties of microalgae: the effect of cell size and cell wall, *Appl. Opt.*, 46, 5762–5769, 2007.
- Taguchi, S.: Relationship between photosynthesis and cell size of marine diatoms, *J. Phycol.*, 12, 185–189, 1976.
- Thinh, L.-V.: Effect of irradiance on the physiology and ultrastructure of the marine cryptomonad, *Cryptomonas* strain Lis (Cryptophyceae), *Phycologia*, 22, 7–11, 1983.
- Toon, O. B. and Ackerman, T. P.: Algorithms for the calculation of scattering by stratified spheres, *Appl. Opt.*, 20, 3657–3660, 1981.
- Twardowski, M. S., Boss, E., Macdonald, J. B., Pegau, W. S., Barnard, A.H., and Zaneveld, J. R. V.: A model for estimating bulk refractive index from the optical backscattering ratio and the implications for understanding particle composition in Case I and Case II waters, *J. Geophys. Res.*, 106(C7), 14129–14142, 2001.
- Utermohl, H.: Zur Vervollkommnung der quantitativen Phytoplankton, *Methodik. Mitt. Int. Ver. Theor. Angew. Limnol.*, 9, 1–38, 1958.
- Vaillancourt, R. D, Brown, C. W., Guillard, R. R. L., and Balch, W. M.: Light backscattering properties of marine phytoplankton: relationships to cell size, chemical composition and taxonomy, *J. Plankton Res.*, 26, 191–212, 2004.
- Van de Hulst, H. C.: *Light Scattering by Small Particles*, Wiley, New York, 1957.
- Visviki, I.: A Cytological Study of the Green Alga *Chlamydomonas applanata Pringsheim* (Chlamydomonadaceae), *J. Torrey Bot. Soc.*, 127, 1–8, 2000.
- Volten, H., de Haan, J. F., Hovenier, J. W., Schreurs, R., Vassen, W., Dekker, A. G., Hoogenboom, H. J., Charlton, F., and Wouts, R.: Laboratory measurements of angular distributions of light scattered by phytoplankton and silt, *Limnol. Oceanogr.*, 43, 1180–1197, 1998.
- Whitmire, A. L., Boss, E., Cowles, T. J., and Pegau, W. S.: Spectral variability of the particulate backscattering ratio, *Opt. Express*, 15, 7019–7031, 2007.
- Witkowski, K., Wolinski, L., Turzynski, Z., Gedziorowska, D., and Zielinski, A.: The investigation of kinetic growth of *Chlorella vulgaris* cells by the method of integral and dynamic light scattering, *Limnol. Oceanogr.*, 38, 1365–1372, 1993.
- Witkowski, K., Krol, T., Zielinski, A., and Kuten, E.: A light-scattering matrix for unicellular marine phytoplankton, *Limnol. Oceanogr.*, 43, 859–869, 1998.

Phytoplankton optical models with two layered spheres

S. Bernard et al.

Title Page

Abstract

Introduction

Conclusions

References

Tables

Figures

◀

▶

◀

▶

Back

Close

Full Screen / Esc

Printer-friendly Version

Interactive Discussion



Yentsch, C. S.: Measurement of visible light absorption by particulate matter in the ocean, *Limnol. Oceanogr.*, 7, 207–217, 1962.

Zaneveld, J. R. V., and Kitchen, J. C.: The variation in the inherent optical properties of phytoplankton near an absorption peak as determined by various models of cell structure, *J. Geophys. Res.*, 100(C7), 13309–13320, 1995.

5

Zaneveld, J. R. V.: A theoretical derivation of the dependence of the remotely sensed reflectance on the inherent optical properties, *J. Geophys. Res.*, 100(C7), 13135–13142, 1995.

BGD

6, 1497–1563, 2009

**Phytoplankton
optical models with
two layered spheres**

S. Bernard et al.

Title Page

Abstract

Introduction

Conclusions

References

Tables

Figures

◀

▶

◀

▶

Back

Close

Full Screen / Esc

Printer-friendly Version

Interactive Discussion



Phytoplankton optical models with two layered spheres

S. Bernard et al.

Table 1. Relative chloroplast volume (Vv in %) for a range of cultured phytoplankton species under varying growth conditions. The paucity of published data regarding chloroplast morphology has necessitated the use of different methods to generate chloroplast volume data, as given by the Vv methods column. The upper box represents cultures considered low light ($<200 \mu\text{E m}^{-2} \text{s}^{-1}$), and the lower box high light ($>200 \mu\text{E m}^{-2} \text{s}^{-1}$). Where necessary growth illuminance quoted in lux have been converted with $1 \mu\text{E m}^{-2} \text{s}^{-1} = 60 \text{ lux}$. EVSD=equivalent volume spherical diameter, Av =relative area, d =diameter, TEM=transmittance electron micrograph.

Species	Class	EVSD (μm)	Vv (%)	No. Chloroplasts	Light ($\mu\text{E m}^{-2} \text{s}^{-1}$)	Vv Method	Reference
<i>Phaeodactylum tricornutum</i>	Bacillariophyte	2.2	20.7	two large	5	Av quoted/ d from TEM	Janssen et al. 2001
<i>Phaeodactylum tricornutum</i>	Bacillariophyte	2.2	8.9	two large	50	Av quoted/ d from TEM	Janssen et al. 2001
<i>Nannochloropsis</i>	Eustigmophyte	2.7	57.0	one large	35	Vv quoted	Fisher et al. 1998
<i>Aureococcus anophagefferens</i>	Pelagophyte	2.8	12.5	one large	unknown	TEM spheroidal geometry	Pitcher et al. 1999
<i>Pavlova pinguis</i>	Haptophyte	3.6	14.9	one large	unknown	TEM spheroidal geometry	Green 1980
<i>Amphidinium carterae</i>	Dinophyte	4.3	26.4	one large	unknown	Vv quoted	Jenks and Gibbs 2000
<i>Cryptomonas lis</i>	Cryptophyte	4.9	25.8	two large	10	Av quoted	Thinh 1983
<i>Chlamydomonas applanata</i>	Chlorophyte	5.1	52.0	one large	30	Vv quoted	Visviki 2000
<i>Cyclotella cryptica</i>	Bacillariophyte	5.7	19.8	several	5	Av quoted/ d from TEM	Janssen et al. 2001
<i>Cyclotella cryptica</i>	Bacillariophyte	6.4	4.4	several	50	Av quoted/ d from TEM	Janssen et al. 2001
<i>Symbiodinium spp</i>	Dinophyte	8.1	17.0	many	50	Vv quoted	Muller-Parker et al. 1996
<i>Symbiodinium spp</i>	Dinophyte	8.1	33.0	many	5	Vv quoted	Muller-Parker et al. 1996
<i>Cyclotella meneghiniana</i>	Bacillariophyte	16.1	21.5	several	10	Vv quoted	Janssen et al. 2001
<i>Cyclotella meneghiniana</i>	Bacillariophyte	16.1	28.6	several	107	Vv quoted	Rosen and Lowe 1984
<i>Glennodiniopsis steinii</i>	Dinophyte	16.8	24.8	one large	155	Vv quoted	Highfill and Pflester 1992
<i>Nannochloropsis</i>	Eustigmophyte	2.7	29.0	one large	650	Vv quoted	Fisher et al. 1998
<i>Amphidinium carterae</i>	Dinophyte	4.3	16.7	one large	unknown	Vv quoted	Jenks and Gibbs 2000
<i>Cryptomonas lis</i>	Cryptophyte	7.3	7.6	two large	260	Av quoted	Thinh 1983
<i>Diatoma tenue</i>	Bacillariophyte	7.8	16.0	several	200	Vv quoted	Sicko-Goad and Stoermer 1979

Title Page

Abstract

Introduction

Conclusions

References

Tables

Figures

◀

▶

◀

▶

Back

Close

Full Screen / Esc

Printer-friendly Version

Interactive Discussion

Phytoplankton optical models with two layered spheres

S. Bernard et al.

Table 2. Published values of the real part of the refractive index for a range of cellular structures from terrestrial plants and algae, relative to water. The mean values for chloroplasts (including those for thylakoid membranes, pigment bound proteins, and light harvesting complexes) are calculated with the highest and lowest values excluded, whilst the mean value for external cellular membranes excludes values for calcite coatings (these are considered specific to the coccolithophore case). RI=refractive index, LHC=light harvesting complex.

Organism/Organelle	RI Value (1+ ϵ)	Method	Reference
Spinach/chloroplast	1.065–1.199	Photovoltage	Paillotin et al. 1998
Spinach/chloroplast	1.030–1.060	Immersion/refractometer	Bryant et al. 1969
<i>A. carterae</i> /chloroplast	1.199	Forster transfer	Kleima et al. 2000
<i>Rb. sphaeroides</i> /LHC II	1.220	<i>In vitro</i> absorption shift	Anderrson et al. 1991
Spinach/chloroplast	1.130	<i>In vitro</i> absorption shift	Renge et al. 1996
Maize/chloroplast	1.150–1.179	Forster transfer	Cinque et al. 2000
<i>Zea Mays</i> /chloroplast	1.124	<i>In vitro</i> absorption shift	Caffarri et al. 2001
<i>Secale cereale</i> /LHC II	1.150–1.390	<i>In vitro</i> absorption shift	Gruszecki et al. 1999
<i>C. pyrenoidosa</i> /chloroplast	1.060	Phase contrast	Charney and Brackett 1961
<i>Chlorella</i> /chloroplast	1.080	Mueller matrix	Quinby-Hunt et al. 1989
General/chlorophyll	1.140–1.150	Lorentz molecular weight	Aas 1996
General /protein	1.132–1.199	Literature review	Aas 1996
Modelled cell/chloroplast	1.095	assumed model value	Zaneveld and Kitchen 1995
<i>C. pyrenoidosa</i> /cytoplasm	1.015	Phase contrast	Charney and Brackett 1961
Modelled cell/cytoplasm	1.020	assumed model value	Kitchen and Zaneveld 1992
Modelled cell/cytoplasm	1.015	assumed model value	Bricaud et al. 1992
<i>Chlorella</i> /cell membrane	1.130	Mueller matrix	Quinby-Hunt et al. 1989
Modelled cell/calcite coating	1.220	assumed model value	Bricaud et al. 1992
Modelled cell/cell membrane	1.090	assumed model value	Zaneveld and Kitchen 1995
Algal/carbohydrate forms	1.162	Literature review	Aas 1996
Mean chloroplast value	1.136 (± 0.053)		
Mean cytoplasm value	1.017 (± 0.003)		
Mean membrane/coating value	1.127 (± 0.036)		

Title Page

Abstract

Introduction

Conclusions

References

Tables

Figures

◀

▶

◀

▶

Back

Close

Full Screen / Esc

Printer-friendly Version

Interactive Discussion



Phytoplankton
optical models with
two layered spheres

S. Bernard et al.

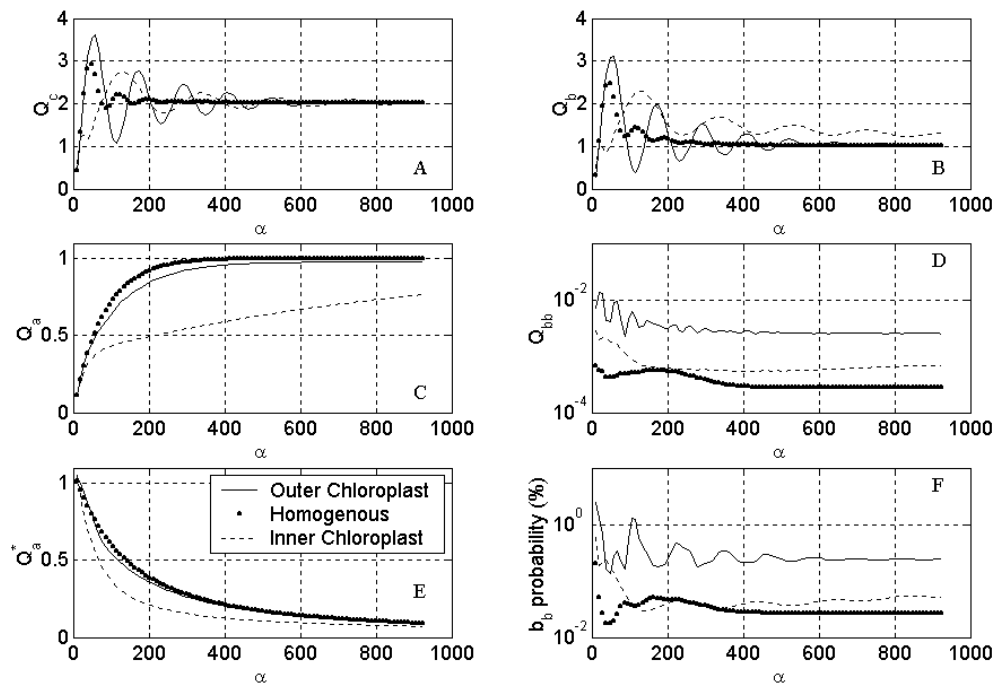


Fig. 1. Optical efficiency factors and backscattering probability against Mie size parameter α for two-layered and homogenous spheres. **(A)** attenuation efficiency factor Q_c , **(B)** scattering efficiency factor Q_b , **(C)** absorption efficiency factor Q_a , **(D)** backscattering efficiency factor Q_{bb} , **(E)** package effect parameter Q_a^* , **(F)** backscattering probability factor $b_{b\phi}$. Two-layered spheres in both inner (dashed line) and outer (solid line) chloroplast configurations have refractive indices of $m_{\text{chlor}}=1.14-0.02i$ and $m_{\text{cyto}}=1.02-0.0005i$. Homogenous spheres (dots) have a refractive index of $m_{\text{h}}=1.044-0.0044i$, calculated as volume equivalent to the two-layered geometry using Gladstone-Dale equivalence. Relative chloroplast volume is set to 20%. Note the log scales for the two backscattering related graphs.

Title Page

Abstract

Introduction

Conclusions

References

Tables

Figures

◀

▶

◀

▶

Back

Close

Full Screen / Esc

Printer-friendly Version

Interactive Discussion



Phytoplankton optical models with two layered spheres

S. Bernard et al.

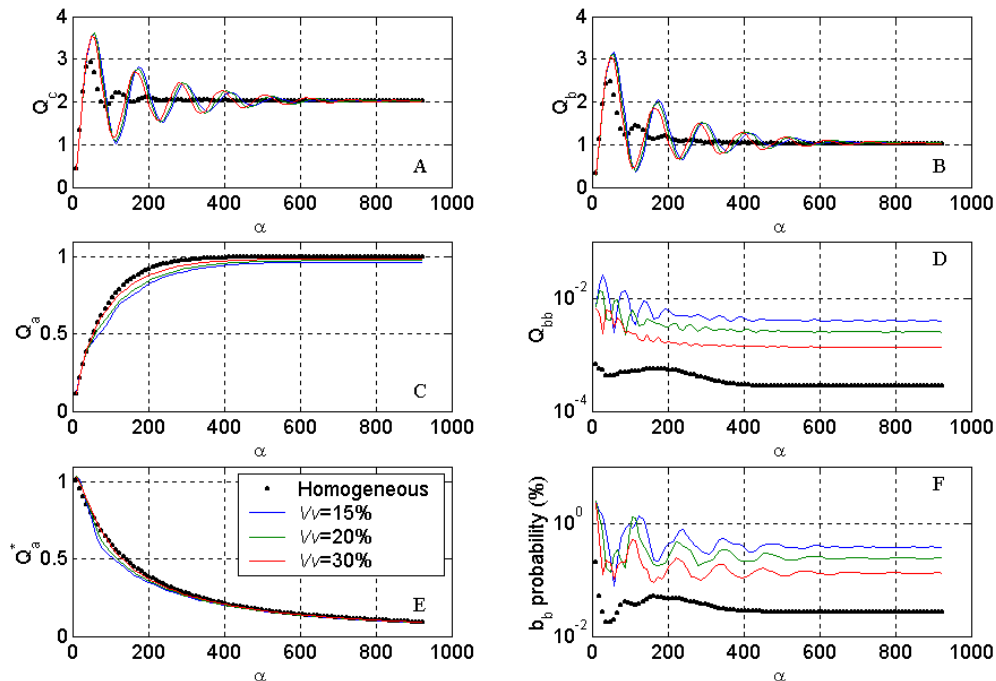


Fig. 2. Optical efficiency factors and backscattering probability against Mie size parameter α for homogeneous spheres and heterogeneous spheres of varying relative chloroplast volume Vv and volume equivalent refractive indices. **(A)** attenuation efficiency factor Q_c , **(B)** scattering efficiency factor Q_b , **(C)** absorption efficiency factor Q_a , **(D)** backscattering efficiency factor Q_{bb} , **(E)** package effect parameter Q_a^* , **(F)** backscattering probability factor $\tilde{b}_{b\phi}$. Relative chloroplast volumes are set to 15% (blue), 20% (green) and 30% (red). Homogeneous spheres (dots) have a refractive index of $m_h=1.044-0.0044i$. Two-layered spheres (lines) with an outer chloroplast configuration have volume equivalent refractive indices of $m_{cyto}=1.02-0.0005i$ and $m_{chlor}=1.18-0.0265i$ ($Vv=15\%$), $m_{chlor}=1.14-0.020i$ ($Vv=20\%$) and $m_{chlor}=1.10-0.0135i$ ($Vv=30\%$).

Title Page

Abstract Introduction

Conclusions References

Tables Figures

Navigation arrows

Navigation arrows

Back Close

Full Screen / Esc

Printer-friendly Version

Interactive Discussion



Phytoplankton optical models with two layered spheres

S. Bernard et al.

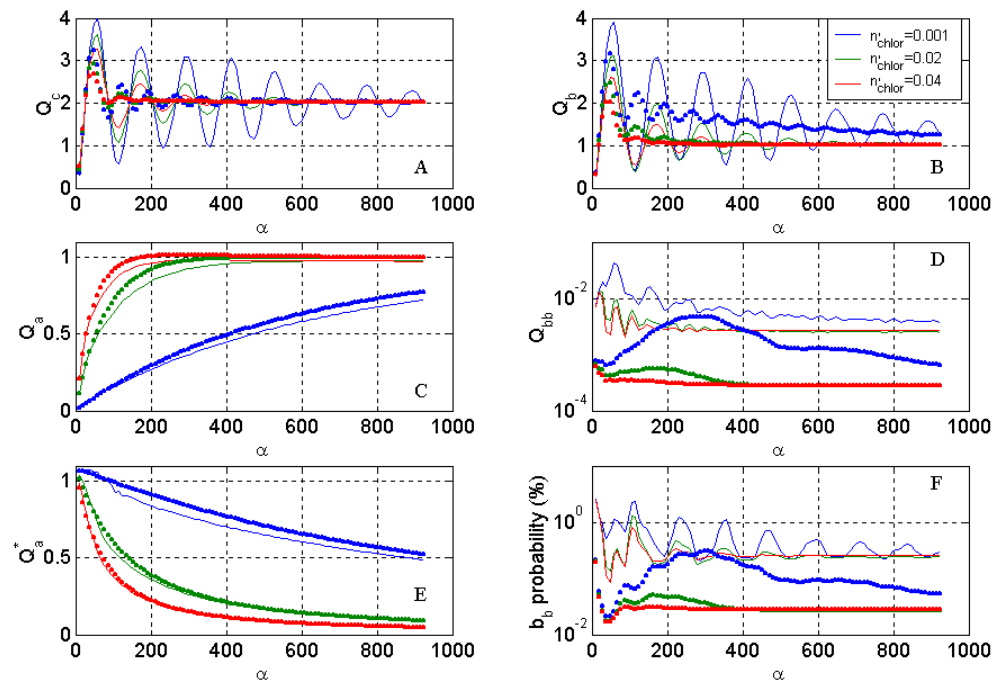


Fig. 3. Optical efficiency factors and backscattering probability against Mie size parameter α for two-layered and homogeneous spheres with varying imaginary part of the chloroplast refractive index. **(A)** attenuation efficiency factor Q_c , **(B)** scattering efficiency factor Q_b , **(C)** absorption efficiency factor Q_a , **(D)** backscattering efficiency factor Q_{bb} , **(E)** package effect parameter Q_a^* , **(F)** backscattering probability factor $b_{b\phi}$. Two-layered spheres (lines) with an outer chloroplast configuration have refractive indices of $m_{\text{cyto}}=1.02-0.0005i$, $n_{\text{chlor}}=1.14$, and n'_{chlor} values of 0.001 (blue), 0.02 (green) and 0.04 (red). Homogeneous spheres (dots) have volume equivalent refractive indices of $m_h=1.044-0.0006i$, $m_h=1.044-0.0044i$, and $m_h=1.044-0.0084i$, respectively. Note the log scales for the two backscattering related graphs.

Title Page

Abstract

Introduction

Conclusions

References

Tables

Figures

◀

▶

◀

▶

Back

Close

Full Screen / Esc

Printer-friendly Version

Interactive Discussion



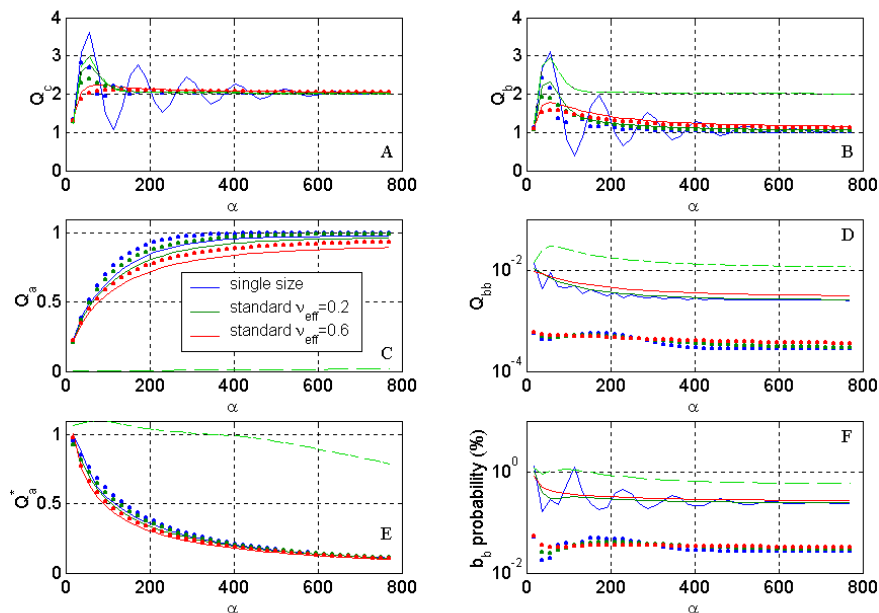


Fig. 4. Optical efficiency factors and backscattering probability against Mie size parameter α for size distributions of two-layered and homogenous spheres with varying polydispersity. **(A)** attenuation efficiency factor Q_c , **(B)** scattering efficiency factor Q_b , **(C)** absorption efficiency factor Q_a , **(D)** backscattering efficiency factor Q_{bb} , **(E)** package effect parameter Q_a^* , **(F)** backscattering probability factor $b_{b\phi}$. Two-layered spheres (lines) with an outer chloroplast configuration have refractive indices of $m_{\text{cyto}}=1.02-0.0005i$, and $m_{\text{chlor}}=1.14-0.02i$. Homogenous spheres (dots) have volume equivalent refractive indices of $m_h=1.044-0.0044i$. Data are shown for a single size (blue), a narrow Standard size distribution with $v_{\text{eff}}=0.2$, and a wide Standard size distribution with $v_{\text{eff}}=0.6$. Note the log scales for the two backscattering related graphs, and the α scale of 1 to 800. The green dashed lined represents a standard size distribution of two-layered spheres with $v_{\text{eff}}=0.2$, $m_{\text{cyto}}=1.02-10^{-5}i$, and $m_{\text{chlor}}=1.14-10^{-5}i$, and demonstrates the effects of low imaginary refractive index in both chloroplast and cytoplasm.

Title Page

Abstract

Introduction

Conclusions

References

Tables

Figures

◀

▶

◀

▶

Back

Close

Full Screen / Esc

Printer-friendly Version

Interactive Discussion



Phytoplankton
optical models with
two layered spheres

S. Bernard et al.

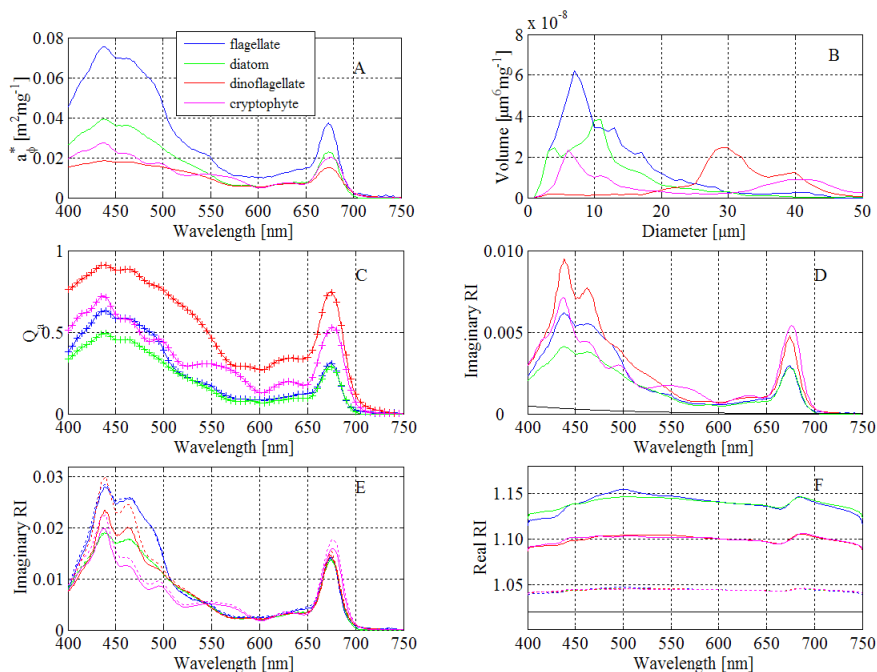


Fig. 5. Optical and size data for four sample algal assemblages. **(A)** Chl-*a*-specific phytoplankton absorption, **(B)** Chl-*a* specific cellular volume distributions, **(C)** experimental (line) and two layer model values (+) for absorption efficiency factors, **(D)** imaginary refractive indices for homogeneous cells $n'_h(\lambda)$ and for cellular cytoplasm $n'_{\text{cyto}}(\lambda)$ (black line), **(E)** imaginary refractive indices for chloroplasts $n'_{\text{chlor}}(\lambda)$, determined with the inverse Aden–Kerker model (solid line) and from homogeneous values with volume equivalence (dashed lines), **(F)** real refractive indices for chloroplasts $n_{\text{chlor}}(\lambda)$ (solid lines), and volume equivalent homogeneous cells (dashed lines). Note that larger V/V values of 30% were required for successful two-layered Q_a simulation for the two assemblages dominated by larger cells; the dinoflagellate and cryptophyte samples.

Title Page

Abstract

Introduction

Conclusions

References

Tables

Figures

◀

▶

◀

▶

Back

Close

Full Screen / Esc

Printer-friendly Version

Interactive Discussion



Phytoplankton
optical models with
two layered spheres

S. Bernard et al.

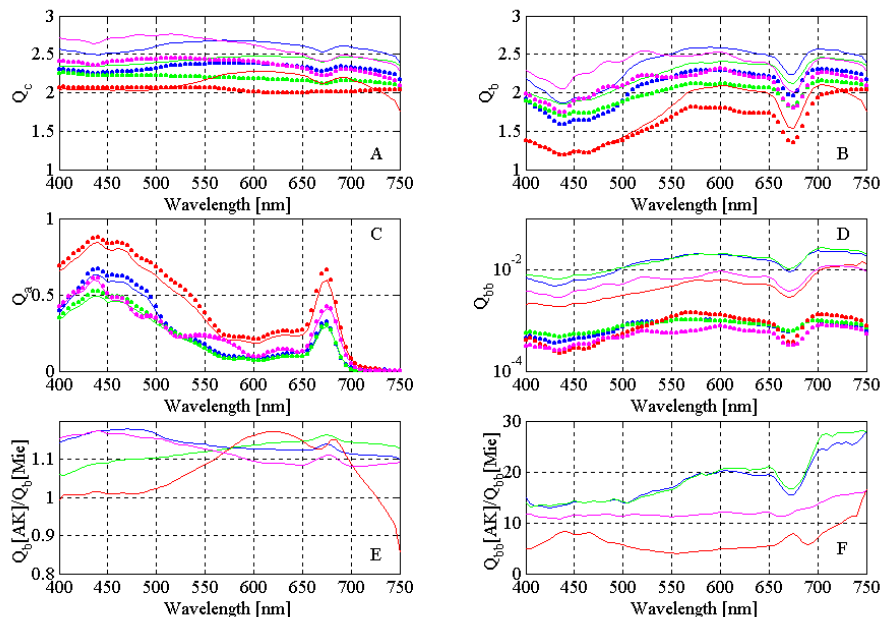


Fig. 6. Optical efficiency factors for the four sample algal assemblages. Legend colours are as for the previous figure, for data from the two-layered geometry (lines) and homogeneous geometry (dots). **(A)** attenuation efficiency factors Q_c , **(B)** scattering efficiency factors Q_b , **(C)** absorption efficiency factors Q_a , **(D)** backscattering efficiency factors Q_{bb} , **(E)** ratio of Q_b for two-layered and homogeneous geometries, **(F)** ratio of Q_{bb} for two-layered and homogeneous geometries. Homogeneous refractive indices are calculated from volume equivalence to the two-layered data to facilitate comparison.

Title Page

Abstract

Introduction

Conclusions

References

Tables

Figures

◀

▶

◀

▶

Back

Close

Full Screen / Esc

Printer-friendly Version

Interactive Discussion



Phytoplankton
optical models with
two layered spheres

S. Bernard et al.

Title Page

Abstract

Introduction

Conclusions

References

Tables

Figures

◀

▶

◀

▶

Back

Close

Full Screen / Esc

Printer-friendly Version

Interactive Discussion

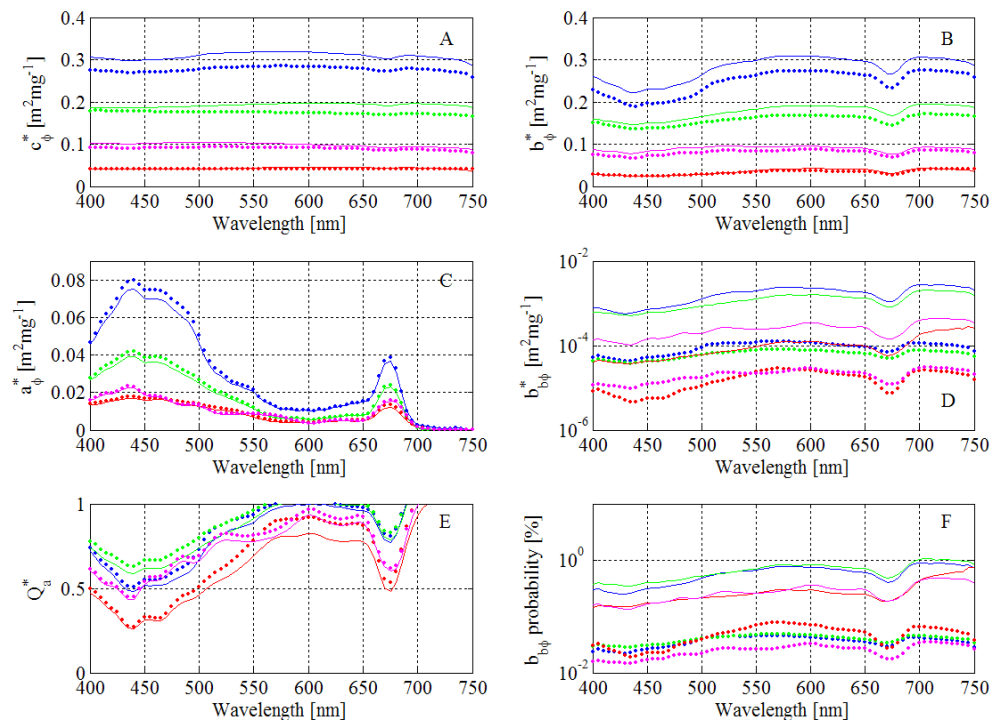


Fig. 7. Chl-*a*-specific inherent optical properties, package effect parameter and backscattering probability data for the four sample algal assemblages. Legend colours are as for the previous figure, for data from the two-layered geometry (lines) and homogeneous geometry (dots). **(A)** Chl-*a*-specific attenuation coefficient $c_{\phi}^*(\lambda)$, **(B)** Chl-*a*-specific scattering coefficient $b_{\phi}^*(\lambda)$, **(C)** Chl-*a*-specific absorption coefficient $a_{\phi}^*(\lambda)$, **(D)** Chl-*a*-specific backscattering coefficient $b_{b\phi}^*(\lambda)$, **(E)** package effect parameter $Q_a^*(\lambda)$, **(F)** Algal backscattering probability factor $\tilde{b}_{b\phi}(\lambda)$. Homogeneous refractive indices are calculated from volume equivalence to the two-layered data to facilitate comparison.

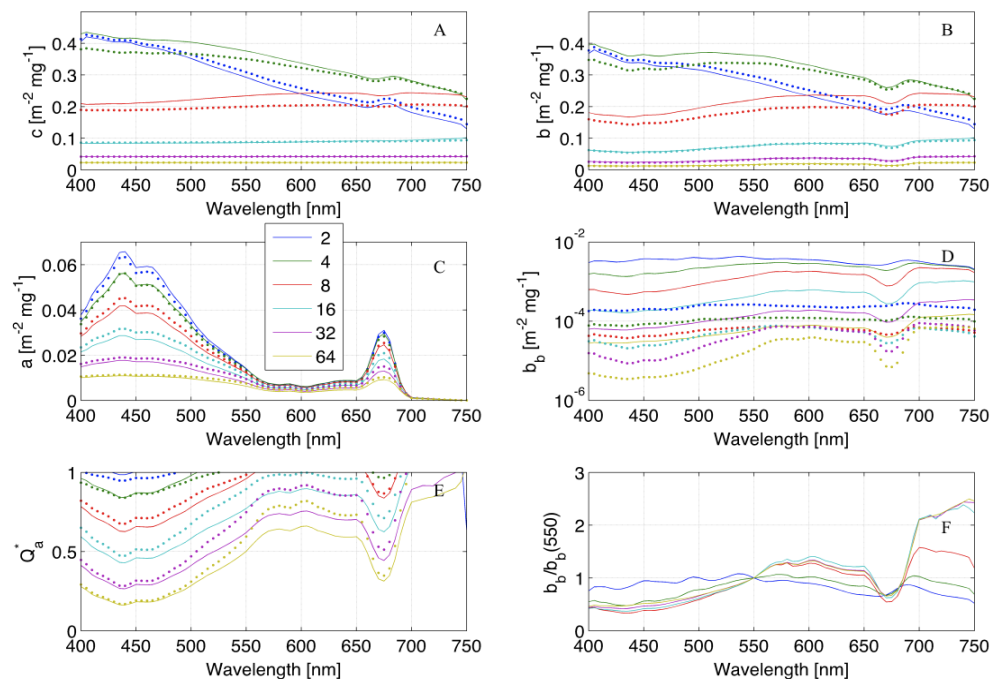


Fig. 8. Chl-*a*-specific inherent optical properties, package effect parameter and backscattering spectral shape data for Standard size distributions of varying d_{eff} and constant $v_{\text{eff}}=0.2$, based upon diatom refractive index data. Effective diameter values (μm) are given in the legend for data from the two-layered geometry (lines) and homogeneous geometry (dots). Figures are **(A)** Chl-*a*-specific attenuation coefficient $c_{\phi}^*(\lambda)$, **(B)** Chl-*a*-specific scattering coefficient $b_{\phi}^*(\lambda)$, **(C)** Chl-*a*-specific absorption coefficient $a_{\phi}^*(\lambda)$, **(D)** Chl-*a*-specific backscattering coefficient $b_{b\phi}^*(\lambda)$, **(E)** package effect parameter $Q_a^*(\lambda)$, **(F)** Algal backscattering coefficient normalised to 550 nm. Homogeneous refractive indices are calculated from volume equivalence to the two-layered data to facilitate comparison, with $c_l=2.3 \text{ kg m}^{-3}$ and $V\nu=20\%$.

Title Page

Abstract

Introduction

Conclusions

References

Tables

Figures

◀

▶

◀

▶

Back

Close

Full Screen / Esc

Printer-friendly Version

Interactive Discussion



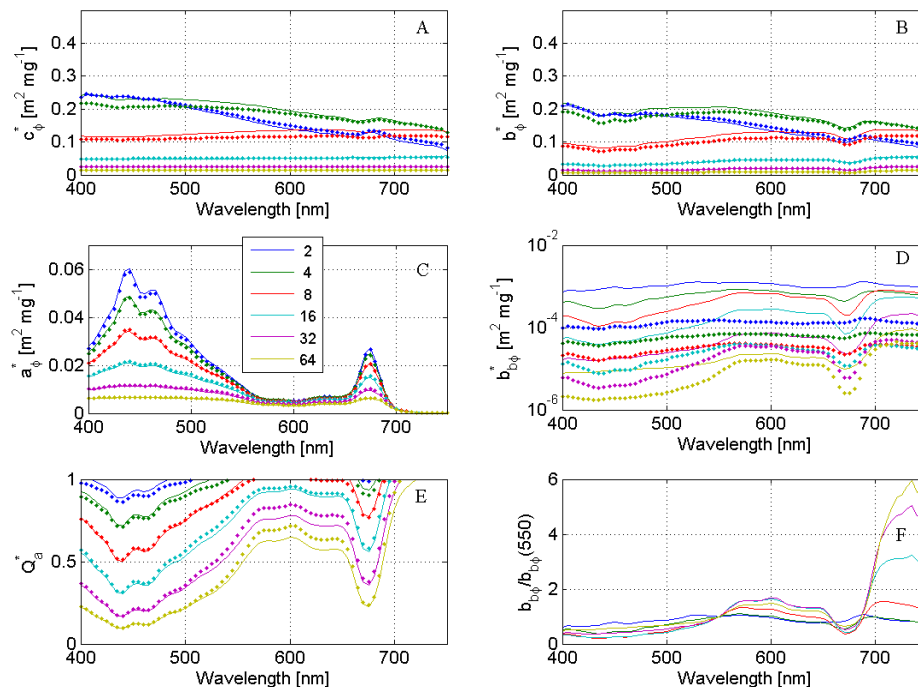


Fig. 9. Chl-*a*-specific inherent optical properties, package effect parameter and backscattering spectral shape data for Standard size distributions of varying effective diameter, based upon dinoflagellate refractive index data. Effective diameter values (μm) are given in the legend for data from the two-layered geometry (lines) and homogeneous geometry (dots). **(A)** Chl *a*-specific attenuation coefficient $c_{\phi}^*(\lambda)$, **(B)** Chl-*a*-specific scattering coefficient $b_{\phi}^*(\lambda)$, **(C)** Chl-*a*-specific absorption coefficient $a_{\phi}^*(\lambda)$, **(D)** Chl-*a*-specific backscattering coefficient $b_{b\phi}^*(\lambda)$, **(E)** package effect parameter $Q_a^*(\lambda)$, **(F)** Algal backscattering coefficient normalised to 550 nm. Homogeneous refractive indices are calculated from volume equivalence to the two-layered data to facilitate comparison, with $c_j = 4 \text{ kg m}^{-3}$ and $V/V = 30\%$.

Title Page

Abstract

Introduction

Conclusions

References

Tables

Figures

◀

▶

◀

▶

Back

Close

Full Screen / Esc

Printer-friendly Version

Interactive Discussion



Phytoplankton optical models with two layered spheres

S. Bernard et al.

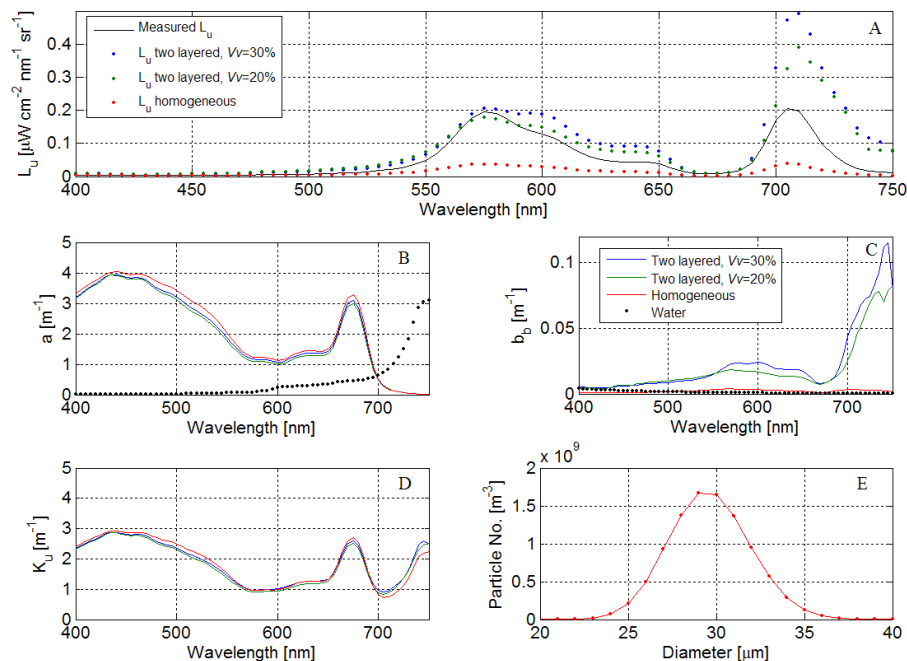


Fig. 10. Comparison of measured and simulated upwelling radiance L_u for an *Alexandrium catenella* bloom with cell concentrations of $9.8 \times 10^6 \text{ cells l}^{-1}$. **(A)** Measured and simulated upwelling radiance L_u for various geometries, **(B)** Simulated algal absorption coefficients and the absorption coefficient of pure water, **(C)** Simulated algal backscattering coefficients and the backscattering coefficient of pure seawater, **(D)** Diffuse attenuation coefficient for upwelling radiance K_u , used to propagate measured L_u to the air-sea interface, and **(E)** Microscope derived algal size distribution.

Title Page

Abstract

Introduction

Conclusions

References

Tables

Figures

◀

▶

◀

▶

Back

Close

Full Screen / Esc

Printer-friendly Version

Interactive Discussion



Phytoplankton
optical models with
two layered spheres

S. Bernard et al.

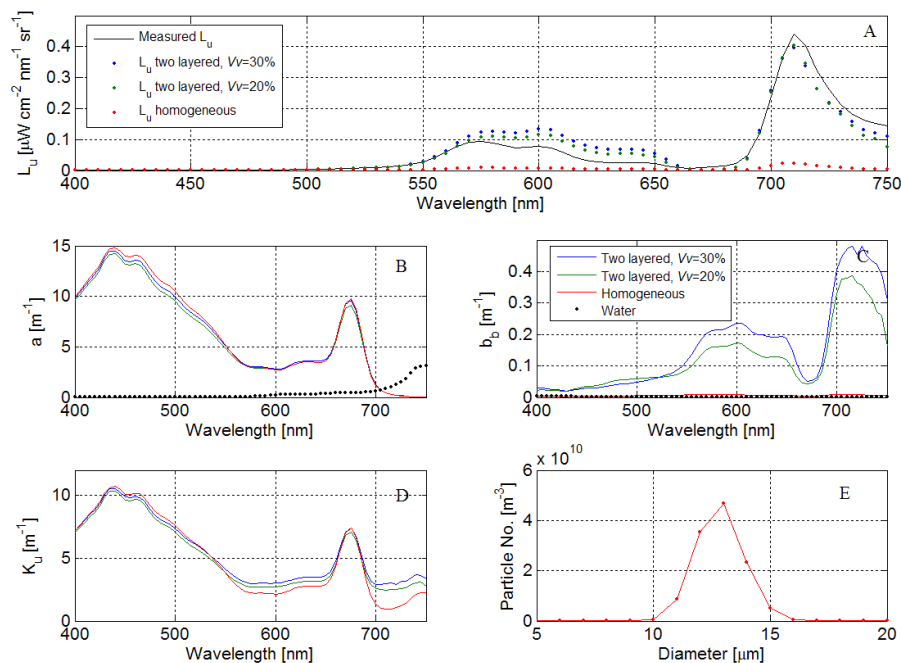


Fig. 11. Comparison of measured and simulated upwelling radiance L_u for a *Prochlorococcus triestinum* bloom with cell concentrations of 1.2×10^8 cells/litre. **(A)** Measured and simulated upwelling radiance L_u for various geometries, **(B)** Simulated algal absorption coefficients and the absorption coefficient of pure water, **(C)** Simulated algal backscattering coefficients and the backscattering coefficient of pure seawater, **(D)** Diffuse attenuation coefficient for upwelling radiance K_u , used to propagate measured L_u to the air-sea interface, and **(E)** Microscope derived algal size distribution.

Title Page

Abstract

Introduction

Conclusions

References

Tables

Figures

◀

▶

◀

▶

Back

Close

Full Screen / Esc

Printer-friendly Version

Interactive Discussion

